A COMPARATIVE STUDY OF PAPER HOLD DOWN SYSTEMS FOR X-Y PLOTTING INSTRUMENTS

By

NWOSU, Edwin Ugochukwu
HND. (Yaba tech), PGD. (Akure)
MAT No. PHY/98/1827

JUNE, 2010

A COMPARATIVE STUDY OF PAPER HOLD DOWN SYSTEMS FOR X-Y PLOTTING INSTRUMENTS

By

NWOSU, Edwin Ugochukwu
HND. (Yaba tech), PGD. (Akure)
MAT No. PHY/98/1827

A DISSERTATION IN THE DEPARTMENT OF PHYSICS, SUBMITTED TO THE SCHOOL OF POSTGRADUATE STUDIES IN PARTIAL FULFILLMENT OF THE REQUIREMENT FOR THE AWARD OF MASTER OF TECHNOLOGY (M.Tech) DEGREE IN PHYSICS (ELECTRONIC MEASUREMENT AND INSTRUMENTATION OPTION) OF THE FEDERAL UNIVERSITY OF TECHNOLOGY, AKURE, ONDO STATE, NIGERIA.

CERTIFICATION

Certification by the Student:

This work has not been presented elsewhere for the award of a degree, or any other purpose.

Candidate's Name: NWOSU E.U. **Signature**..... **Date**.....

Certification by the Supervisors.

We certify that this work was carried out by Mr. NWOSU, Edwin Ugochukwu under supervision in the department of Physics, School of Science, federal University of Technology, Akure.

Supervisor's Name	Signature	Date
(a). DR. BABALOLA M. T (Major Supervisor)	.....	8/10/2010
(b). DR. AJAYI O.S (Co-Supervisor)	.....	.....

ACKNOWLEDGEMENT

My greatest thanks and appreciation go to God Almighty, who saw me through this project work especially all the journeys that I had made during the programme.

I wish to express my sincere gratitude to my supervisor Dr. M. T Babalola for his counsel, support and contributions toward the successful completion of the project.

I am also very grateful to Dr. Osiele for his support especially during thesis registration. My thanks also go to Mr. Ewetumo and Dr. Oseni O.A for support and contributions towards the successful completion of the project.

Finally, my sincere thanks and appreciation go to my wife, Basila and my children, Okwuchukwu and Ifesinachukwu for their prayer, understanding and support throughout the duration of the program.

DEDICATION

This project work is dedicated to God the Father, the Son and the Holy Ghost, by whose grace this work came to a successful conclusion and to my wife and children.

ABSTRACT

A comparative study of the vacuum hold-down system and the electrostatic hold-down system for X-Y plotter was carried out using fabricated prototype units. The vacuum hold-down system consists of a motor driven suction unit, suction chamber, perforated flat plotting surface and pulse-width-modulated motor speed controller. A 24V dc air blower was converted to an air suction unit with an adjustable pump speed controlled by a pulse-width-modulated motor speed controller. The hold-down force on the plotting paper for varying pump speed was measured using gravitational force technique. The graphical analysis (using linear regression) of the collected data produced a linear relationship between the measured hold-down force and the pump speed which showed that the hold-down force is 0.004±0.0001N 5% per 100rpm.

The fabricated electrostatic paper hold down system consists of the electrostatic charging unit, insulated charged metal sheet and flat plotting surface. The design of the electrostatic charging unit was based on voltage multiplication principle with a symmetrical Cockcroft-Walton half wave voltage multiplier circuit (modified Jacob's ladder circuit) powered by a high frequency ac voltage source (500V, 12kHz) obtained using dc-ac voltage inverter circuit. The parallel plate capacitor and the corona discharge methods were used for charging the insulated plate. The hold-down force on the plotting paper for varying charge voltage was measured using gravitational force technique. The experiment showed that the measured force varied linearly with the charging voltage with an average hold-down force of 0.003±0.0001N V^{-1}. The two systems under study

were efficient as paper hold-down systems but the vacuum system was more bulky and it required additional hardware for its implementation.

TABLE OF CONTENTS

LIST OF TABLES

LIST OF FIGURES

CHAPTER ONE

1.0 INTRODUCTION

Instrumentation as it relates to the different fields of science and engineering usually involves the measurement and control of variables which are either modified or retained in a particular state in order to achieve a particular goal in a given system. Many methods are available for the presentation of the data, which usually, are measured with various types of indicating instruments depending on the purpose of data collection, though quite often, a simple mechanical indication is adequate (Austin, 1962).

Instruments are vital especially in the study of the dynamic behaviour of the parameters of different equipment, machines, system's components and materials. Even more vital is the means of collecting and recording the experimental data especially when the data output is directly generated in graphical form.

In circuit development for electrical and electronic systems, the study of the characteristics of active devices usually forms the first step towards its useful application as a circuit element. This is usually accomplished through point-by-point measurement of the parameters of the device (voltage, current, resistance) or by sweep display of its input/output characteristics (Bruce and James, 1969).

In linear circuits and devices, this is achieved via the use of a set of parameters (z, y, h) relating the various terminal voltages and currents. However, in non-linear devices, this single set of numbers becomes inadequate in describing the

electrical characteristics of these devices. The graphical display of the characteristics using such instruments as cathode ray oscilloscope, curve tracer and x-y recorder has been found to be necessary (Bruce and James, 1969).

Sweep displays usually involve the sweeping of one variable through a given range of values, resulting in a complete display of the graphical relationship of the variables involved. In many instances, a permanent record in graphical form is required by an engineer or equipment designer to aid in the analysis of the performance of a system (Laycock, 1976). For a certain range of frequencies, a camera, attached to an oscilloscope or the use of a storage oscilloscope can yield the desired result. But in situations where greater accuracy and higher resolution than is obtained with an oscilloscope are desired, the x-y recorder is employed to produce the required graphical display on conventional graph paper (Bruce and James, 1969).

The same result can also be achieved using a data logging device. This involves the collection and recording of data under the control of a computer. Thereafter the collected data can be stored in the permanent memory or other storage devices, displayed on screens as tables, graphs or charts or the information is printed on paper in graphical or tabular form depending on the type of analysis carried out on the collected data.

Plotting/recording instruments employ direct-writing technique on circular or rectangular-strip charts in the presentation of experimental data accomplished by the movement of the plotting pen in two or three orthogonal directions in response to electrical signals applied at its inputs (Laycock, 1976). For most

direct-writing instruments, the paper is drawn at a constant speed from the paper spool but for the X-Y plotter which involves the cross-plotting of one variable against another, the plotting paper is held stationary on the plotting surface by means of magnetic strips, suction force or electrostatic attraction while two independently controlled servo motors (or stepper motors) move the pen in the horizontal (X-axis) and the vertical (Y-axis) directions respectively (Haslam, 1993). The three methods of holding the paper stationary are based on simple principles of physics. This project work focuses on two of them namely the vacuum technique and the electrostatic technique.

The vacuum technique utilizes the pressure produced when a chamber is evacuated while the electrostatic effect results from the force of attraction between oppositely charged metal plates. The two physics concepts have wide areas of industrial application.

1.1 Objective

The aim of this project is to carry out a comparative study on two paper hold down systems used by X-Y plotter instruments: the electrostatic paper hold down system and the vacuum paper hold down system. The study will involve comparing their operation principles and ease of implementation. This will involve the fabrication of prototypes of the paper holding devices with which the study will be carried out. The effectiveness and efficiency of the devices in accomplishing the task of holding plotting paper on the plotting area of the X -Y plotter will then be computed.

CHAPTER TWO

2.0 LITERATURE REVIEW

2.1 Problems and uses static electricity

To many engineers and scientists, static electricity only brings to memory images of the ancient Van de Graaff generator and hair-rising experiments usually seen in science museums and documentaries. But at one time or another, one must have had a firsthand experience of the everyday harmless manifestation of static electricity such as the shock sensation felt on touching metallic door handle during dry harmattan weather and the paper scraps that are attracted by a piece of amber that has first been rubbed on the sleeve (Taylor and secker, 1994).

However, these harmless manifestations of static electricity are minor effects compared with problems usually associated with the same effect in industries which often times results in production loss. An example is the electrostatic cling, where plastic or textile fibers wrap themselves round rollers of conveyor systems or product guides which very frequently results in line shutdowns (Taylor and secker, 1994).

The problem associated with static electricity is also experienced in the semiconductor industry where it causes immense production loss. Electrostatic discharge usually occurs when a charge imbalance exists between an integrated circuit chip and another object. Moving parts from place to place during manufacturing and distribution of semiconductor devices is the main cause for developing this charge imbalance. Also the devices come into contact with

people and moving machines during the process. This charge imbalance is mainly caused by triboelectric charging, a charging process that occurs when two dissimilar materials rub together and then separate. For instance, when a single IC chip slides down an insulative rail guide during production, a charge imbalance is generated; which very often leads to electrostatic discharge. This may lead to the eventual failure of the device due to induced high current densities and electric fields resulting from the electrostatic discharge occurrence (Vinson and Liou, 1998).

The above problems notwithstanding, electrostatic effect has many areas of application which include: electrostatic painting, electro-photography (photocopy machines), smoke detectors, non-impact printers and electret pickups used for microphone outputs (Taylor and Secker, 1994).

Also in printing, film and foil production industries, electrostatic systems are a vital part of the production process where the control and creative use of the static electricity has added to the quality, efficiency and profitability of the industries.

2.2 The vacuum hold-down system

The pressure difference between two surfaces or the pressure of fluid particles moving at different speeds within a given medium produces a force of varying magnitude which has been put into many useful applications in science and engineering. An example is the suction force as applied in the use of straw for sipping liquid from bottles. Domestic and industrial vacuum cleaners are other

applications of suction force due to air particles moving at different speeds within a given container.

The relationship between pressure and velocity at different parts of a moving compressible fluid such as air was derived by Bernoulli in 1740. He established that when velocity of a mass of moving air increases, there is a corresponding decrease in pressure.

This fact is derived from the conservation of energy and involves the kinetic energy of the moving mass of air and the potential energy stored due to the 'springiness' of that air. Pressure (p) which is defined as force per unit area can also be expressed as energy per unit volume:

$$\textit{Energy per unit volume} = p \quad \ldots\ldots\ldots\ldots\ldots\ldots\ldots\ldots\ldots\ldots\ldots\ldots 2.1$$

A moving mass of air has kinetic energy given as:

$$\textit{kinetic energy per unit volume} = \frac{1}{2}\rho v^2 \quad \ldots\ldots\ldots 2.2$$

where ρ =air density and v = velocity of air.

Combining equations 2.1 and 2.2 gives the mechanical energy possessed by the mass of moving air.

$$\textit{Total mechanical energy per unit volume} = p + \frac{1}{2}\rho v^2 \quad \ldots\ldots\ldots\ldots 2.3$$

The total mechanical energy per unit volume is constant if the non-mechanical forms of energy such as chemical reactions, heat, and friction are ignored. The total energy given by equation 2.3 above only applies to streamline motion of a non-viscous incompressible fluid with no frictional force opposing the motion of the fluid.

Bernoulli's principle shows that at any point in a moving fluid where the potential energy change is very small, pressure is low where the velocity is high and high where velocity is low. The maximum pressure usually occurs at a point where the air velocity is zero. This point is referred to as stagnation point and the pressure as stagnation pressure. The principle has many applications which include: suction effect (force due to partial vacuum), filter pump and aerofoil lift (Cornish, 1987).

2.3 Electromechanical devices (fans)

Electromechanical devices (fans) utilizing mechanical energy of a rotating impeller are used to produce controlled movement of air mass and differential air pressure for ventilating and cooling systems (McPherson , 1993). These devices, also known as low pressure air pump utilize power from an electric motor to output a volumetric flow of air at a given pressure, whereby a propeller (impeller) converts the torque from the motor to increased static pressure across the fan rotor as well as the kinetic energy of the air particles (Turner and Rotron, 2004).

Their uses include domestic and industrial applications such as: air circulation in rooms and buildings for cooling/heating systems; cooling of motors, materials and products; extraction of dust and noxious fumes; conveying of light materials; forced draft in steam boilers and heating, ventilating and air-conditioning systems (Gudavaili et al, 2003).

For affecting the air flow, the fan develops a total pressure difference between the inlet and outlet air streams. This total rise in pressure in the air streams is made of two components namely:

i. Static pressure which depends on the aerodynamic characteristics of the fan impeller such as blade profile, the number of blades, its blade angle, hub shape.

ii. Dynamic pressure developed due to the kinetic energy imparted to the air stream. It is the pressure that corresponds to the average velocity of the air mass at the fan outlet.

2.3.1 Classification of fans

One characteristic by which fans are classified is the nature of the flow through the blade passages; axial flow, radial flow, mixed flow, and cross flow are all possible in fan impellers. Propeller fans, tube-axial fans, and vane-axial fans all make use of axial flow impellers (Avallone and Baunmeister, 1987). A second classification is based on the mechanical design. In this classification, fans are put in groups namely centrifugal and axial fans (McPherson, 1993). Centrifugal fans, often referred to as "squirrel cage" fans resemble a paddle wheel and operate on the principle of "throwing" air away from the blade tips.

Air enters near the centre (eye) of the impeller, turns through a right-angle and moves radially outward by the centrifugal action between the blades of the rotating impeller.

Figure 2.1: Types of centrifugal impeller blades

The blades may be straight or backward curved or forward curved with respect to the direction of rotation. Each design produces a distinctive performance characteristic.

2.3.1.1 Centrifugal fans

Centrifugal fan impellers have a number of blades around their periphery which

rotate in a scroll or volute shaped casing. As the impeller rotates, air is thrown from the blade tips centrifugally into the snail shell shaped casing and out through the discharge opening, and at the same time more air is drawn into the 'eye' of the impeller through a central inlet opening of the fan thus creating a continuous flow of air through the fan impeller between the air inlet and outlet. Centrifugal fans with backward-curved blades are generally more efficient than those with forward-curved and straight blades. They are used in applications where high airflow rates and high static pressures are required. Centrifugal fans with forward-curved blades have somewhat lower static pressure capabilities but tend to be quieter than the other blade designs. An advantage of the straight blade design is that with proper design it can be used to handle dirty air or convey light materials. Dust collectors and silage blowers are examples of straight-blade centrifugal fans (Bodman and Shelton, 1996). Forward-curved

blades are shallow and curved so that both the tip and the heel point in the same direction of rotation. Radial and radial tip blades are both radial at the tip, but the latter is curved at the heel to point in the direction of rotation. Backward-curved and backward-inclined blades point in the direction of rotation at the heel and in the opposite direction at the tip. All the types of blade described above are of uniform thickness and are designed for radial flow. The pressure producing capability of radial flow fans varies with blade depth, tip speed and blade angle. The blade angle is a function of the number of blades on the fan impeller.

2.3.1.2 Axial Fans

Axial fans operate on the same principle as an aircraft propeller, but the number of impeller blades varies for different applications. In a typical axial fan, the air movement is straight through the impeller at a constant distance from the axis. The primary component of blade force on the air is directed axially from inlet to outlet and thus provides the pressure rise by a direct blade action. The blade force necessarily has an additional component in the tangential direction, providing the reaction to the driving torque: this sets the air spinning about the axis independent of its forward motion.

The air delivering capacity of axial flow fans ranges from 3 to 14,000 cubic metres per minute. Their impellers usually have blades with cross-sections matching those of an aerofoil. Compared to curved sheet blades, an aerofoil can apply greater force to the air, thereby increasing maximum pressure and maintaining better efficiency over a wider range of volumetric flow. Also by

increasing the thickness and curvature of the inner sections, the blades are made stiffer; which limits flutter and allows the impellers to be run at higher speeds.

Axial fan impellers rotate at a higher blade tip speed than a centrifugal fan of similar dimension and, hence, tend to be noisier. They also suffer from a pronounced stall characteristic at high resistance. However, they are more compact, can easily be combined into series and parallel configurations and can produce reversal of the airflow by changing the direction of impeller rotation, although with reduced efficiency (Robert, 1987).

A great deal of the energy is transferred in axial flow fans in form of kinetic energy. Some of this kinetic energy can be transformed into pressure energy by reducing the exit velocity using a diffuser (Robert, 1987). Axial-flow fans are further classified based on their construction and performance characteristics into: propeller fan, tube-axial fan and vane-axial fan.

2.3.1.3 Propeller Fans

Propeller fans are commonly used for ventilating livestock buildings. Their basic design enhances their ability to remove dust and dirt accumulations. They normally consist of a "flat" frame or housing for mounting a propeller-shaped blade, and a drive motor. Propeller fans effect very little transformation and hence have very low pressure producing capacity (Robert, 1987).

Tube-axial fans are fans made up of tube-shaped housing, propeller-shaped blades, and a drive motor.

Vane-axial fans are a variation of tube-axial fans. Both are similar in design and application. The major difference is that air straightening vanes are added either in front or behind the blades which results in a slightly more efficient fan, capable of greater static pressures and airflow rates (Robert, 1987).

2.4 LAWS FOR FAN OPERATION

The fan laws are useful in predicting their performance when certain operating parameters are varied and geometrically similar fan operation performance can be characterized by the following equations:

$$Volumetric\ airflow(G) = K_q ND^3 \qquad 2.4$$

$$Mass\ flowrate(m) = K_p \rho ND^3 \qquad 2.5$$

$$Pressure = K_p \rho N^2 D^2 \qquad 2.6$$

$$Power\ output(HP) = K_{HP} \rho N^3 D^5 \qquad 2.7$$

where: K = constant for geometrically and dynamically similar operation, N = fan speed in RPM, D = fan diameter, ρ = air density.

From the equations, the following laws can be deduced:

1. Both the air volumetric flowrate and mass flowrate in m^3/s are directly proportional to the fan speed.
2. Change in the total pressure (Δ P in N/m^2) is proportional to the square of the fan speed.

3. The shaft power P (in kW or HP) required for driving the fan is proportional the cube of the fan speed.

However, every fan design has its own characteristic curve, which is a graph made by plotting a number of test points showing volume delivered against air resistance.

The curves enable the user to calculate the amount of air the fan will move under different conditions. In its simplest form, the curves are a plot of the volume of air moved in m^3/s against air resistance (static pressure) in Pascal.

The curves obtained are similar, irrespective of the fan type (either axial or mixed flow or centrifugal) but the horizontal and vertical scales differs for differing impeller diameters of similar fans.

Each curve is obtained by collecting a series of data points from the instruments on a test rig. The starting point is to measure the airflow at zero pressure, sometimes referred to as Free Inlet and Discharge (FID). The test rig is then adjusted to increase the pressure that the fan has to work against and the airflow at each point is measured. It is normally only the "linear" part of the performance curve of that is published as shown in figures 2.2 to 2.4. Figure 2.2 is characteristics curves of an axial fan for different impeller blade angles. The volume of air moved decreases with the angle of the impeller but the speed of rotation of the fan impeller remains theoretically constant.

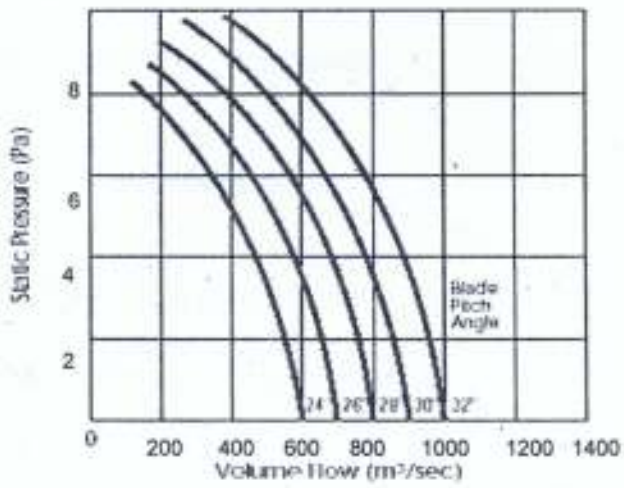

Figure 2.2: Graph of fan static pressure versus air flow for different blade pitch angles.

Fiqure 2.3 shows the fan dynamic pressure or velocity pressure curve while figure 2.4 shows the total pressure curve

The dynamic pressure is calculated as follows:

$$Dynamic\ \Pr essure = 0.5\, x\, \rho\, x Velocity^2 \qquad 2.10$$

where ρ *is* the density of the air in kg/m^3 and the velocity is in m/s.

the total pressure is the arithmetic addition of the static pressure and the dynamic pressure.

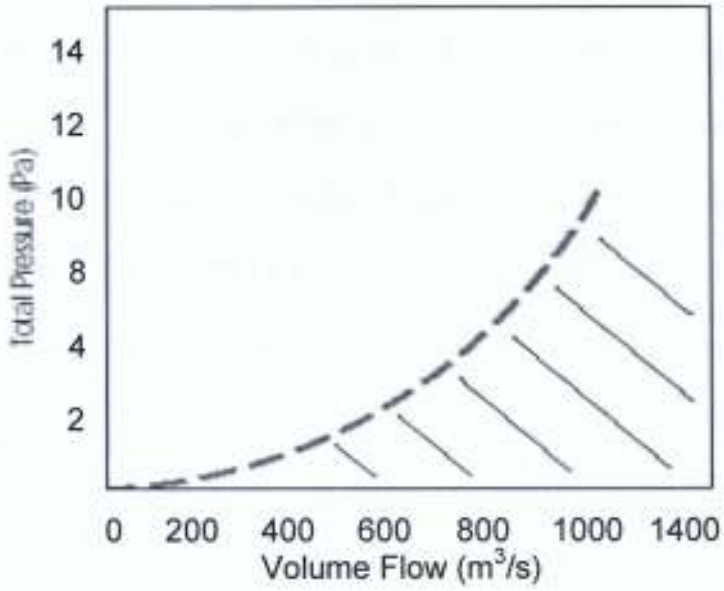

Figure 2.3: Graph showing the fan dynamic pressure characteristics curve

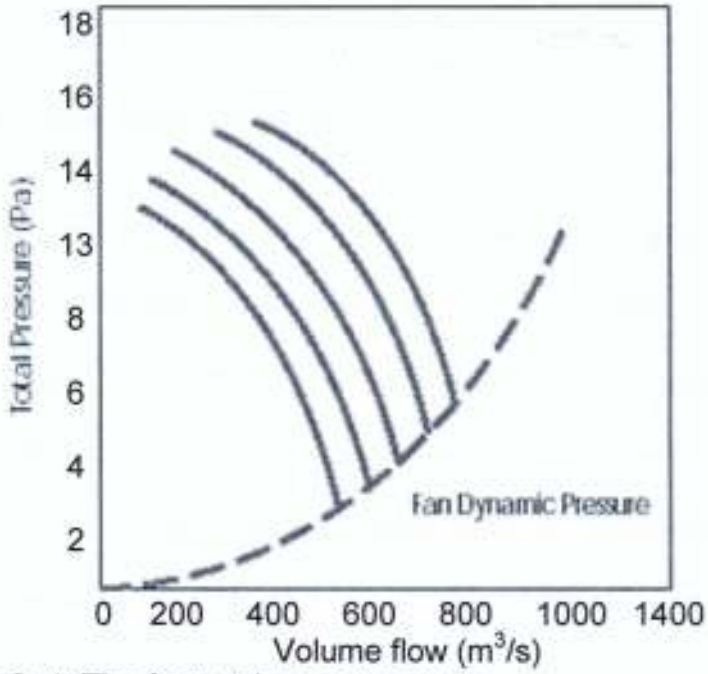

Fig.2. 4: The fan total pressure curve

2.5 ELECTROSTATIC CHARGING

Electrostatic charging provides a method of temporarily attracting or holding materials in place by means of the force of attraction between two opposite electric charges. For instance, stacks of paper or plastic materials can be virtually "glued" together temporarily by an electrostatic charging system as shown in fig.2-5. The materials are later separated by discharging them or by allowing the electrostatic charge to wear off.

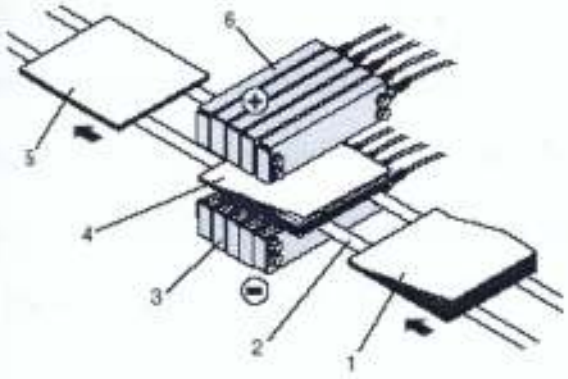

1. Unbounded paper
2. Rail guide
3. negative charging electrodes
4. paper under charge
5. temporary bounded paper
6. positive charging electrodes

Fig. 2-5 temporary paper adhesive system

Though most materials are electrically neutral having equal quantities of positive and negative charges, forces between two electrically charged objects can be extremely large when the bodies carry large quantities of charge. Nearly all electrostatic phenomena are caused by the interaction between charges located on the surfaces of bodies or materials which may be conductive as well as insulative (Jonassen, 2000).

According to Coulomb's law, the electrostatic force between two charged particles is directly proportional to the product of the magnitudes of the charges and inversely proportional to the square of the distances between the charges.

The resultant force between two charges q_1 and q_2 is given by;

$$\underline{F} = \frac{1}{4\pi\varepsilon_0}\frac{q_1 q_2}{r^2}\hat{r} \qquad 2.9$$

where $\hat{r}$ is a unit vector in the direction of r.

When q_1 is negative, and q_2 is positive the force is attractive. When both are of the same sign, the force is repulsive.

This means that opposite charges attract and like charges repel.

It is important however to stress that these charges are never generated. They exist in atoms as positive charges on the protons of the nuclei, and as negative charges on the electrons around the nuclei but their electrostatic effect is only seen when electrons are removed from the atoms in one material and transferred to atoms in another material.

And the effect is manifested if the electron-exchanging materials are separated in such a manner that the charges do not reunite during the separation process. The transfer of electrons between atoms or molecules might occur when two solids contact each other, with electrons crossing the interface in a preferential direction, giving one material a positive charge and the other a negative charge causing an imbalance in the atomic species of the materials (Jonassen, 2000).

Electrostatic charging can be by contact, friction, induction and the quantity of charge transferred is usually very enormous (Taylor and Secker, 1994).

For example, between 100,000 to 1 million electrons are transferred when a powder, such as sugar or flour, slides down a tube and its tiny particles stick to

the wall of the tube. Each particle contains about 10^{-14} to 10^{-13} coulombs of charge and a plastic folder rubbed with a piece of cloth or fur typically produces 10^{-7} C of charge (Jonassen, 2000).

Generally, electrostatic charge build-up occurs as a result of an imbalance of electrons on the surface of a material. This imbalance of electrons produces an electric field that can be measured and that can influence other objects nearby (EDSA, 2000).

2.5.1 Charging by Contact and Friction

At the basic level charging by contact and friction is a simple process. Two different but electrically neutral materials when in contact, charge transfer from one surface to the other takes place to bring the materials into charge equilibrium with equal but opposite charges. The surfaces retain their charges if they are quickly separated and isolated from earth after the charging process.

Charging by contact here describes simple contact between two surfaces i.e charging in which no sliding or rubbing occurs between the two contacting surfaces. Charging by contact occurs with all materials (metals, insulator or polymers) with varying charge retention capacities after separation. For contacts between good conducting surfaces, the charge retained on breaking the contact is usually small because charges flow to the last point of contact where they recombine. The charge retention capacity of the material is improved if the surfaces are spherical though the transferred charge is still reduced by back-tunneling or back-discharge effects (Taylor and Secker, 1994).

Where one or both of the materials are insulators, the charges are trapped on or inside the insulator surface making charge separation much more efficient though the overall efficiency is affected by back-tunneling and back discharge effects.

Simple non-rubbing contacts are rare because contacting surfaces come together in a way that makes a certain degree of rubbing inevitable. However, experiments have shown that when an insulating surface is rubbed either by a conductor or another insulator, charge transfer is much greater than in simple non rubbing contact. This is because rubbing increases the intimacy of the contacting surfaces. Supporting evidence for this view has been provided by Coste and Pechery (1981) who showed that charge transfer was greatest when surface roughness was small and Haenan (1976) who showed that charge transfer increases with rubbing pressure. Generally, increasing the speed of rubbing also increases the quantity of charges transferred during the charging process (Montgomery, 1959). Instances have also shown that the magnitude of charges generated varies with the speed of rubbing (Ohara, 1979) as well as changes in the polarities of the generated charges (Zimmer, 1970). These effects were attributed to local temperature gradient across the contacting surfaces resulting in enhanced charge diffusion from the hotter surface to the cooler surface.

2.5.2 Triboelectric charging

Two dissimilar materials can become charged with equal but opposite charges due to contact and separation (Greason, 1987). For example, amber can acquire an electric charge by contact and separation (or friction) with a material like wool.

This involves the transfer of electrons between the objects in which one object gaining electrons on its surface becomes negatively charged, and another object losing electrons from its surface, becomes positively charged. When two solid materials, A and B, contact and possibly rub against each other, electrons could move across the interface.

After coming into contact, a chemical bond (adhesion) is formed between the two surfaces, with charges moving from material A to B to equalize their electrochemical potential. This creates the net charge imbalance between the objects as shown in fig. 2.7. On separation, atoms of B acquires extra electron giving away by atoms of A. Figure 2.6 shows atoms of two electrically neutral materials "A" and "B" with equal numbers of protons and electrons before contact.

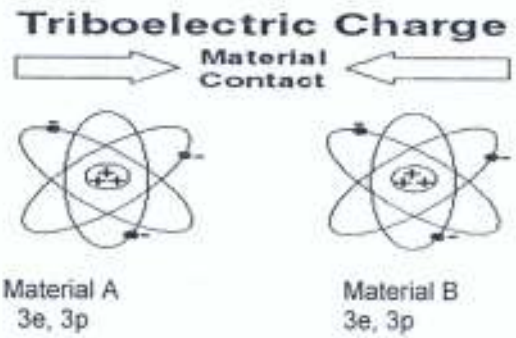

Fig. 2.6 Triboelectric charging mechanism (materials charge distribution before contact

After contact and separation, negatively charged electrons are transferred from the surface of material A to the surface of the material B.

The amount of charge created by triboelectric charging is affected by the area of contact, the speed of separation and relative humidity (ESDA, 2000).

A person can get triboelectrically charged in a number of ways, even by just walking across a carpeted room in dry weather.

The voltage levels of some simple means of static voltage generation are shown in table 2.1.

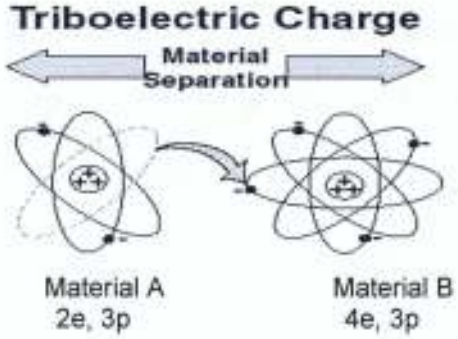

Figure 2.7: The charge distribution in the materials after contact and separation

Table 2.1: Electrostatic effects and generated static voltages for different relative Humidity

Means of Generation	10-25% RH	65-90% RH
Walking across carpet	35,000V	1,500V
Walking across vinyl tile	12,000V	250V
Worker at bench	6,000V	100V
Poly bag picked up from bench	20,000V	1,200V
Chair with urethane foam	18,000V	1,500V

Several mechanisms contribute to the charge generated by the triboelectric process but the following have been identified to have the greatest influence:

- Surface contact effects.
- Work function.
- Charge backflow.
- Gas breakdown.

Surface contact effects include the surface roughness, contact force, and frictional heating caused by rubbing, all of which influence the total surface area of contact between the materials during tribocharging. The greater the surface contact, the greater the resulting net charge is when the two surfaces are separated. Also the smoother the surfaces, the more contact they make with each other and possible increase in the exchange of charges.

Surface-charge imbalance is related to friction because both depend on the adhesion between two surfaces on the molecular level. Two surfaces may stick together because chemical bonds form on the surface. When the surfaces are separated, some bonds may rupture, and any asymmetrical bonds will tend to leave unbalanced charges behind. The surface bonds that rupture depend on their work function.

The work function of a material is the capability of the material to hold its free electrons in its outermost shell. The greater the work function, the less likely it is for the material to give up its free electrons during contact. The weaker the work

function is, the more likely the material will acquire a positive charge by losing some of its free electrons. In general, materials with higher work functions tend to appropriate electrons from materials with lower work functions and the magnitude and polarity of the resultant charge is proportional to the difference in their work functions (Davies, (1969); Greason, (1975).)

$$Q = K(W_1 - W_2) \qquad 2.10$$

where W_1 and W_2 are the appropriate work functions.

This relationship is true especially for metal-insulator contacts, made with clean surfaces, in a high vacuum environment. Though the amount of charge remaining after separation cannot be clearly calculated, it is a function of the materials in contact, the relative movement of surfaces, contact pressure, ambient conditions and surface contaminants (Greason, 1987).

Charge backflow occurs when two materials have been charged and then separated from each other with some of the charges returning to their original materials and reducing the net charge on either surface obtained from tribocharging.

Gas breakdown can occur between two surfaces during separation. The microscopic topology of a surface has many peaks and valleys. One of these peaks may have substantial charge that yields a large electric field in a very small area, causing corona discharge (the breakdown of the air molecules that are acting as insulating medium) between the two separating surfaces.

function is, the more likely the material will acquire a positive charge by losing some of its free electrons. In general, materials with higher work functions tend to appropriate electrons from materials with lower work functions and the magnitude and polarity of the resultant charge is proportional to the difference in their work functions (Davies, (1969); Greason, (1975).)

$$Q = K(W_1 - W_2) \qquad 2.10$$

where W_1 and W_2 are the appropriate work functions.

This relationship is true especially for metal-insulator contacts, made with clean surfaces, in a high vacuum environment. Though the amount of charge remaining after separation cannot be clearly calculated, it is a function of the materials in contact, the relative movement of surfaces, contact pressure, ambient conditions and surface contaminants (Greason, 1987).

Charge backflow occurs when two materials have been charged and then separated from each other with some of the charges returning to their original materials and reducing the net charge on either surface obtained from tribocharging.

Gas breakdown can occur between two surfaces during separation. The microscopic topology of a surface has many peaks and valleys. One of these peaks may have substantial charge that yields a large electric field in a very small area, causing corona discharge (the breakdown of the air molecules that are acting as insulating medium) between the two separating surfaces.

During this breakdown, charge can be transferred from one surface to the other via the plasma path. The amount of charge transferred depends on the distance of separation and the gas pressure.

2.5.2.1 Triboelectric series

One of the parameters that influence the course of the charging process between solid materials is permittivity defined as the ratio of the value of the dielectric displacement to the electric field strength. It is also defined as a measure of the ability of a material to become polarized if placed under the influence of an electric field. A small charged atomic or molecular cluster on an insulative surface is bounded to the surface by polarization forces between the cluster and the surface whose strength depend on the permittivity of the insulative material.

This is the background for Coehn's law, which states that equal and opposite charges are generated on the separation of any two materials in contact and that the substance having the highest dielectric constant becomes positively charged. The law formulated in 1898 was originally based on a comparison of known values of permittivities and published triboelectric series (i.e., a list of materials arranged in such an order that any material will become positively charged when rubbed against another material that is nearer the negative end of the series).

Appendix A shows an example of a triboelectric series a loose ranking of a material's polarity when triboelectrically charged with another material (ESDA,

2000). The series can be used to predict the polarity of the charge that is transferred from one surface to another but they are difficult to reproduce and are only useful for materials well separated in the series (Cross, 1987).

The magnitude of the charges transferred often increases with the degree of friction between the surfaces, and the reason for this could be that the rubbing increases the area of contact between the surfaces while the charging process itself is only governed by the energy state of the surfaces, and that charged particles cross the interface at points of sufficient proximity. This, however, is hardly a satisfactory interpretation, because then it would not be possible to explain the fact that two identical surfaces can get charged by rubbing against each other though It could be argued that no two surfaces are ever identical and that incidental and uncontrollable differences might cause different affinities to charged particles.

2.5.3 Charging by Induction

Charging by induction occurs when an uncharged conductor is grounded while under the influence of an electric field. Charging by induction does not require any physical contact between the charging object and the object being charged.

When an object gets charged by induction, a charge is created by the influence of the charging object though not in contact with it. The word induction means to influence without contact.

A transient current of one polarity will be generated when the conductor is inductively charged by grounding it while under the influence of the electric field. Another transient current of opposite polarity will result if the previously inductively charged body is moved from the influence of the electric field and then discharged by grounding.

Some of the advantages of charging a body by induction include:

- The originally charged object does not lose any charge so it need not be recharged.
- The induced charge can be quite strong.

2.5.4 Corona charging

Corona discharge is a self sustaining, partial breakdown of gas molecules When subjected to a high level of electric field. The American Standard Association defines corona as "a luminous discharge due to ionization of the air surrounding a conductor around which exists a voltage gradient exceeding a certain critical value". This is due to the formation of electron avalanche round the conductor which occurs when the intensity of the electric field at the conductor surface exceeds a critical value due to ionization of air molecules around the region of the conductor.

The field E_p, is given as:

$$E_p = \frac{V}{r} \qquad 2.11$$

V stands for the applied voltage and r the radius of the conductor.

Corona discharge though a product of electrical overstress conditions in many industrial processes, is also one of the methods of electrostatic charging in a number of industrial applications. Notable among this is the electrostatic precipitation of air, dust and smoke where corona discharge is deliberately initiated for the ionization of air molecules and charging of flat metal surfaces for air purification process. In these applications, corona discharge is used as a controlled source of positive and negative electrostatic charges (Taylor and Secker, 1994).

2.5.4.1 Corona charging of flat surfaces

From equation 2.11, the electric field increases with the applied voltage. The increase in the electric field continues until electron avalanche is triggered as in Townsend α-process where electron population grows exponentially as a result of ionizing collision with neutral air molecules. (Taylor and Secker, 1994) For a point-plane electrode geometry shown in figure 2.8, the ionization is confined to the high field region near the point electrode resulting in a highly ionized region characterized by a faint glow whose colour and appearance is dependent on the type of gas and the magnitude and polarity of the applied voltage.

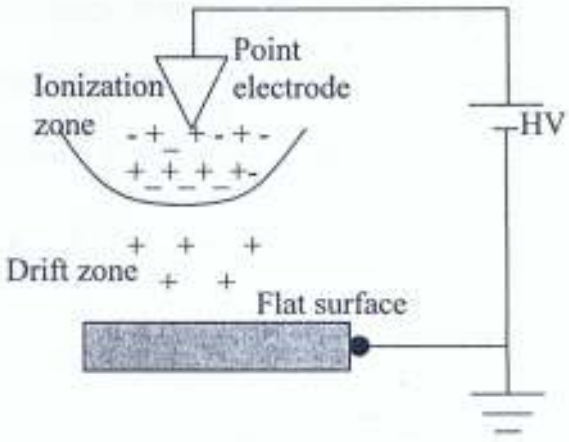

Fig 2.8 Point-plane electrode geometry corona charging mechanism showing the drift and ionization zones

Between the corona point and the plane electrode, two charged zones exist: the ionization zone, close to the corona point and the drift zone near the plane electrode. The presence of both positive and negative ions in the ionization zone results in bipolar current flow within the zone. In the drift zone no ionization takes place. As a result, only single polarity ions repelled from the ionization zone drift into the zone towards the plane electrode. The drifting ions play two important roles within the system.

- Prevents complete electrical failure of the air gap between the electrodes by providing a stabilizing resistance in series with ionization zone.
- Charging any object placed within the drift zone. The charging is due to the interception of ion streams by the object which eventually charges it.

The polarity of the charged object depend the polarity of the voltage applied to the corona electrode. Both positive and negative charging can be effected.

The magnitude of the voltage that will initiate a corona discharge is determined by the thickness of the corona point electrode or wire. The limiting field for corona onset E_c is given as (Taylor and Secker, 1994):

$$E_c = \frac{0.18}{\sqrt{r}} x10^6 \qquad 2.12$$

where E_c is in V/m and r in metres.

Combining equations 2.11 and 2.12 gives the corona threshold voltage as

$$V_c = 1.8x10^5 \sqrt{r} \qquad 2.13$$

Table 2.2 gives corona threshold voltages for different values of r.

r (m)	1.00	0.50	0.10	0.05
V_c (kV)	5.69	4.02	1.80	1.27

In some charging applications as in electro-photography and electrostatic precipitation, the corona source is a thin wire usually made of tungsten. For a wire held coaxially within an earthed cylinder, the limiting electric field is given as (Taylor and Secker, 1994):

$$E_w = \frac{V}{r \ln(\frac{R}{r})} \qquad 2.14$$

where r is the radius of the wire , R the radius of the earthed cylinder and V the applied voltage.

The threshold electric field that will initiate corona discharge is given by Peek (1929) as:

$$E_c = (f\delta)(A + \frac{B}{\sqrt{\delta r}}) \qquad 2.15$$

where A and B are constants given as 3.1×10^6 V/m and 9.55×10^4 V/m respectively. f is the wire roughness factor (< 1) and δ is relative air density and r is in meters.

The threshold voltage for a smooth wire at normal atmospheric pressure approximates to:

$$V_c = \{Ar + B\sqrt{r}\} \ln \frac{R}{r} \qquad 2.16$$

for wires of radius greater than 0.05m. For wires of radius less than 0.05m, Vyverbery (1965) suggested an empirical relation given as:

$$V_c = 2.85 + 34.6r \qquad 2.17$$

For wires placed 12.7mm above an earthed plane. V_c is in kV if r is in mm.

Table 2.3 gives the corona thresholds for two different air gaps calculated from equation 2.17 for smooth wires of different diameters in laboratory air.

Table 2.3 Corona threshold voltages calculated from equation (2.17) for two different air gaps and for wires of different radii.

radius of wire (in mm)	Corona voltage(kV) for R=10mm	Corona voltage(kV) for R=50mm
1.0	14.1	23.9
0.5	11.0	17.0
0.1	5.8	7.9
0.05	4.4	5.7

CHAPTER THREE

3.0 METHODOLOGY

3.1 Design Considerations

This section considers the theoretical analysis of the:

a. Centrifugal fan impeller design that will help in determining the specification of the fan impeller needed for the project together with the rating of the electric motor needed to drive the impeller

b. electrostatic charging system.

3.1.1 The Centrifugal Impeller

Figure 3.1 illustrates a rotating backward bladed centrifugal impeller. Air enters at the impeller eye, turns through a right angle and, as it moves radially outwards, is subjected to a centrifugal force resulting in an increase in its static pressure. Rotational and radial components of velocity are imparted to the air mass. The corresponding outlet velocity is then partially converted into static pressure within the surrounding volute or fan casing.

At any point on a flow path, the velocity may be represented by vector components with respect to the moving impeller. The vector diagram in figure 3.1 is for a particle of air leaving the outlet tip of one impeller blade. The velocity of the air mass relative to the blade is W in the direction tangential to the blade at its tip. The air velocity also has a vector component u in the direction of motion of the tip of the blade. The resultant velocity is C; the radial component of velocity is C_m.

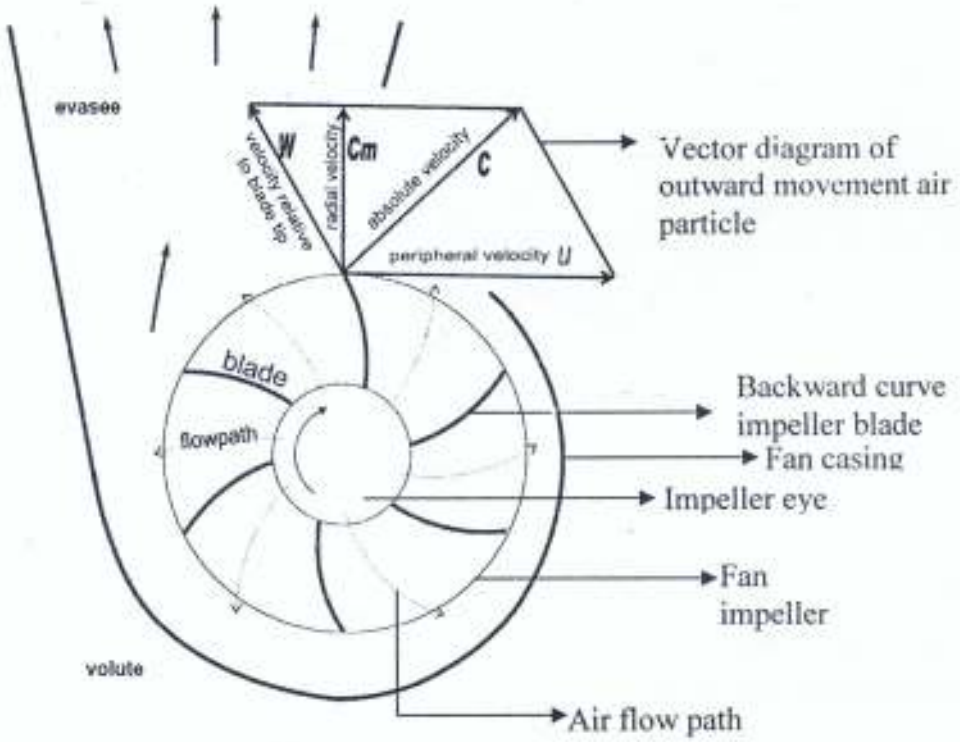

Fig 3-1: Diagram of a centrifugal fan impeller

3.1.2 Theoretical pressure of a centrifugal impeller

Figure 3.2 shows a more detailed diagram of a centrifugal impeller indicating the inlet and outlet vector diagrams for the impeller velocities and forces.

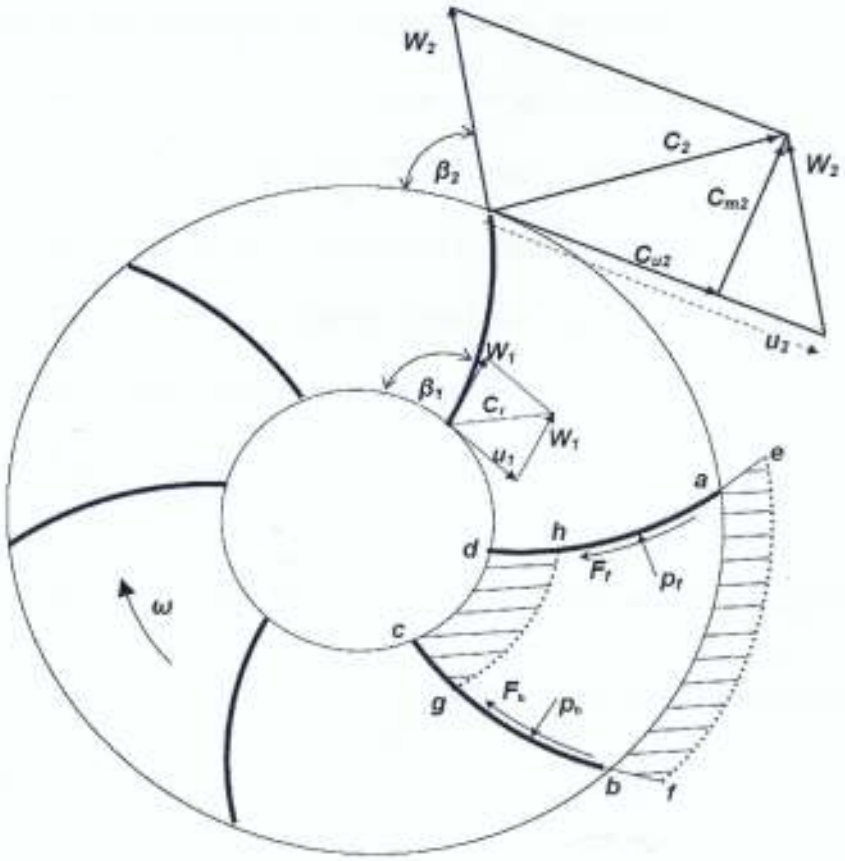

Figure 3-2: Velocities and forces on a centrifugal impeller.

Inlet Parameters

ω : Angular velocity (radians/s)

u : Peripheral speed of blade tip (m/s)

C_m : Radial component of fluid velocity (m/s)

β : Vane angle

pf : Pressure on front of vane (Pa)

Ff : Shear resistance on front of vane (N/m^2)

Outlet parameters

C : Resultant fluid velocity (m/s)

W : Fluid velocity relative to vane (m/s)

C_u : Peripheral component of fluid velocity (m/s)

pb : Pressure on back of vane (Pa)

Fb : Shear resistance on back of vane (N/m^2)

The expression for the pressure developed by the impeller rotational motion of the blade is derived by applying the principle of angular momentum to the volume of air mass moving through the impeller. The pressure relates to the suction force generated by the impeller during its rotational motion.

For a volume of air of mass m rotating about the axis of the impeller blade of radius r and with tangential velocity v, the angular momentum is given as

$$Angular\,momentum = m\omega$$
$$where\,\omega = vr \qquad 3.1$$

And for a continuous movement of the air mass, the mass of air now becomes a mass flow $(\frac{dm}{dt})$, i.e rate of flow of mass. A torque T equal to the corresponding continuous rate of change of momentum is maintained by the impeller motion. The torque is given as:

$$T = \frac{dm}{dt}(rv) \qquad 3.2$$

where r represents the radius of the impeller and v its peripheral velocity.

From figure 3.2, the peripheral velocity is given as C_u and equation 3.2 now becomes

$$T = \frac{dm}{dt}(rC_u) \qquad 3.3$$

If we consider the mass of air filling the space between two blades represented by *abcd* on Figure 3.2, after time dt, it moves to position efgh.

The element abfe leaving the impeller has a mass dm which is equal to the mass of the element cdhg entering the impeller during the same time.

The volume represented by abgh remains in the same position without change in its angular momentum. Any increase in angular momentum is that due to the

elements abfe and cdhg. Applying equation (3.3) across the inlet and outlet locations of the impeller produces a torque T given by:

$$T = \frac{dm}{dt}[r_2 C_{w2} - r_1 C_{w1}] \qquad 3.4$$

Now extending the flow to the whole impeller instead of the two blades, the change of air mass (dm/dt) becomes:

$$\frac{dm}{dt} = Q\rho \qquad 3.5$$

where Q = volume flow (m^3/s) and ρ = fluid density (kg/m^3)

$$T = Q\rho[r_2 C_{w2} - r_1 C_{w1}] \qquad 3.6$$

The power of the impeller is obtained by considering the power of a rotational motion given as the product of its torque and angular velocity. i.e

Power = Impeller torque x angular velocity

But,

$$\begin{aligned} Power &= \frac{energy}{time} \\ &= \vec{F}\, x\, \vec{r}\, x\, \omega \\ &= m\frac{dv}{dt} r\omega \\ &= \frac{d}{dt}(mv) r\omega \\ &= T\omega \end{aligned} \qquad 3.7$$

where ω = speed of rotation (radians/s)

Substituting for T from 3.4, 3.7 becomes

$$P_{ow} = Q\rho\omega[r_2 C_{w2} - r_1 C_{w2}] \qquad 3.8$$

But $\omega r_2 = u_2$ = tangential velocity at outlet

and $\omega r_1 = u_1$ = tangential velocity at inlet, then

$$P_{ow} = Q\rho[u_2 C_{w2} - u_1 C_{w1}] \qquad 3.9$$

But the power imparted by a fan impeller to a volume of air is given by $(P_{fs}Q)$ where P_{fs} is the rise in fan total pressure.

For a streamline non-viscous flow, $P_{fs}Q$ is equal the power consumed by the impeller (P_{ow}), that is

$$P_{fs}Q = Q\rho[u_2 C_{w2} - u_1 C_{w1}] \qquad 3.10$$

and

$$P_{fs} = \rho[u_2 C_{w2} - u_1 C_{w1}] \qquad 3.11$$

Equation 3.11, usually referred to as Euler's equation, gives the expression for evaluating the total pressure for the fan.

The inlet flow is assumed to be radial for an ideal centrifugal impeller, making C_{u1} equal zero and reducing equation 3.11 to:

$$P_{fs} = \rho[u_2 C_{w2}] \qquad 3.12$$

Euler's equation can be re-written in a manner that is more amenable to physical interpretation.

From the outlet vector diagram, we have that:

$$W_2^2 = C_{m2}^2 + (u_2 - C_{w2})^2$$
$$= C_{m2}^2 + u_2^2 - 2u_2 C_{w2} + C_{w2}^2$$

or

$$2u_2 C_{w2} = u_2^2 - W_2^2 + (C_{m2}^2 + C_{w2}^2)$$
$$= u_2^2 - W_2^2 + C_2^2$$

Similarly for the inlet,

$$2u_1 C_{w1} = u_1^2 - W_1^2 + C_1^2$$

Euler's equation 3.12 then becomes,

$$P_{ft} = \rho\{\frac{u_2^2 - u_1^2}{2} - \frac{W_2^2 - W_1^2}{2} + \frac{C_2^2 - C_1^2}{2}\} \qquad 3.13$$

$(\frac{u_2^2 - u_1^2}{2})$ is due to centrifugal effect,

$(\frac{W_2^2 - W_1^2}{2})$ is due to relative velocity of the air molecules and

$(\frac{C_2^2 - C_1^2}{2})$ due to change in kinetic energy of the system.

The total pressure therefore arises from the sum of gains in static velocity and the kinetic energy.

3.2 Electrostatic systems

An electrostatic system may be represented by the simple electrical equivalent circuit in figure 3.3. It consists of four basic elements namely:

- Current generator representing the charge generating mechanism.
- Capacitor (the charge storage device). This may be the surface of an insulating roller, metalwork or personnel not properly earthed.
- Resistance representing the charge relaxation mechanism in an electrically stressed insulator.
- Spark gap that limits the maximum voltage that can be attained in the system.

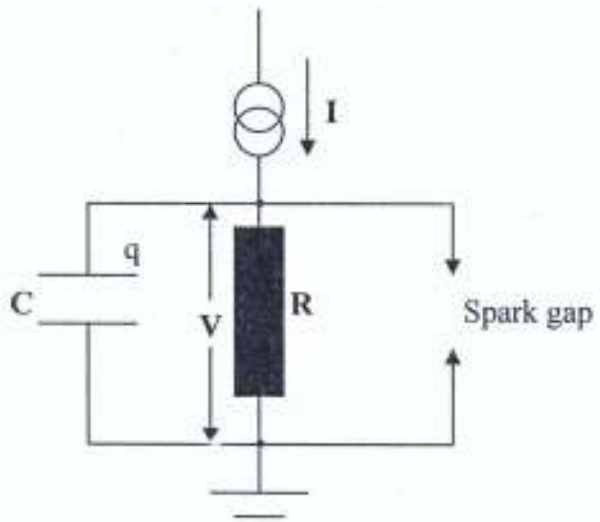

Figure 3.3: An equivalent circuit for an electrostatic system

The electrostatic effect produced by the system depends on the magnitude of the voltage V_e and on the magnitude of the resulting electric field in the insulator across which the voltage appears.

The instantaneous voltage across the capacitor is given by ohms law and reaches an equilibrium value V_e given by

$$V_e = \frac{Q}{C} \qquad 3.15$$

The electrostatic holding system consists of an electrostatic generator and a charge storage device which is made up two parallel conducting plates separated by an insulating medium. The generator, a low power, high voltage system provides the required voltage for the establishment of an electric field for the generation of the electrostatic force required to hold the paper on the plotting surface of the instrument.

It is assumed that the plotting surface is a uniform sheet of charge. The electric field of an infinite uniform sheet of charge, directed normally to the sheet, has a constant value given as:

$$E = \frac{\sigma}{2\varepsilon_r \varepsilon_0} = \frac{\sigma}{2\varepsilon} \qquad 3.16.$$

where σ is the charge density of the sheet and $\varepsilon\varepsilon_0$ is the permittivity of the medium.

This results in a force attracting any object, in this case a sheet of paper, towards its surface. T

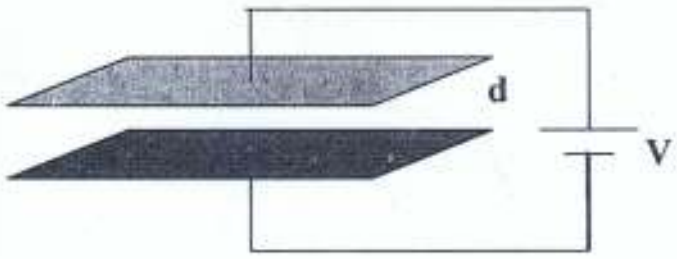

Fig. 3.4 The parallel plate capacitor model

Assuming the plates are made up of neutral atoms, the application of the external potential across the plates initiates a process of charge ionization within the material of the plates and subsequent transfer of charges across the plates whose polarity will depend on the polarity of the applied voltage. The resulting electric field strength is directly proportional the magnitude of the voltage and inversely proportional to the distance between the plates as indicated in equation (3.19). With polarity of applied voltage shown in fig 3.4, positive charges will line up the surface of the upper plate while negative charges will line up the surface of the lower plate.

If the separation between the plates is small compared to the lateral dimensions of the plates, the parallel plate model of fig. 3.4 is considered as uniformly charged sheets with charge densities of +q/A and –q/A for the upper and lower plates respectively. The direction of the field however is toward the lower plate and its magnitude is given by equation (3.16).

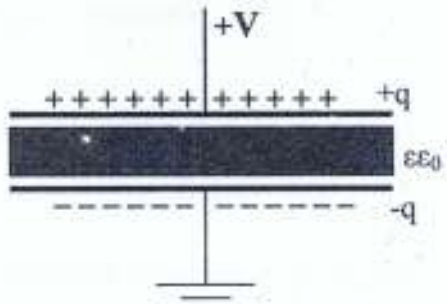

Fig.3.5 equivalent diagram of the capacitor model

The presence of the charges on the surface of the upper and lower plates will result in a force per unit area attracting other charged surfaces towards them depending on their polarities. The magnitude of the force is given by equation 3.18 as:

$$F = \frac{1}{2}\varepsilon\varepsilon_0 E^2$$

Expressing this with respect to the applied voltage and substituting for "E" in eg.3.18 yields

$$F = \frac{1}{2}\varepsilon\varepsilon_0\left[\frac{V}{d}\right]^2 \qquad 3.20$$

3.2.1 Charge Generator

A charge generator is a combination of a high-voltage dc power supply that works in conjunction with charging electrodes (charge applicator) to apply, without physical contact, electrostatic charges to a process or an object. i.e for fixing, positioning or electrostatic "adhesion" of materials.

3.2.2 High Voltage Generator

This uses the principle of voltage multiplication a process of generating high dc voltage with minimal current flow.

Most voltage multiplier circuits, regardless of their topology, consist majorly of rectifiers and capacitors and their operating principle are essentially the same. Capacitors connected in series are charged and discharged on alternate half-cycles of the supply voltage. Rectifiers and additional capacitors are used to force equal voltage increments across each of these series capacitors. The output voltage of a multiplier circuit is simply the sum of these series capacitor voltages. A wide variety of alternating signal inputs is used with multiplier circuits but the most popular are sine and square wave inputs. The output voltage is calculated as:

$$V_O = (n)(V_{in}), \quad as \qquad I_l \to 0 \qquad 3.21$$

where n=number of capacitors, or diodes, assuming equal value capacitors, ideal diodes and symmetrical signal input. In theory, any incremental output voltage can be obtained with increasing value of n but in practice however,

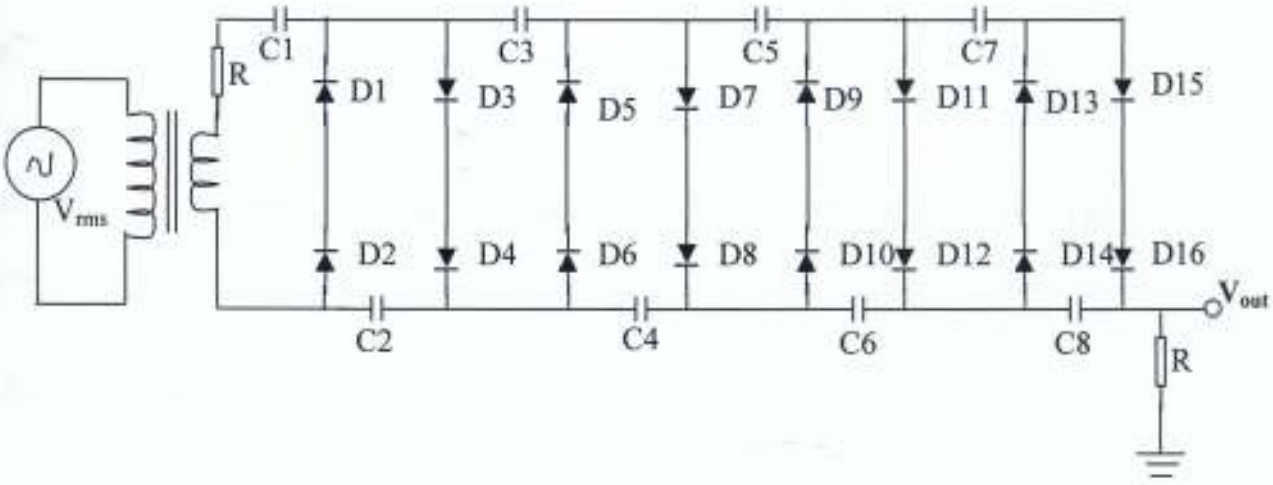

Fig. 3.6 Eight stage voltage multiplier circuit.

voltage regulation and efficiency become increasingly poor as n increases. The voltage multiplier circuit is as shown in figure 3.6.

3.2.2.1 Regulation and ripple calculations

The voltage drop under load can be calculated as (Lux, 2001):

$$V_{drop} = \frac{I_L 2n^2}{fC} \qquad 3.22$$

where I_L is the load current, C is the capacitance per stage, f the frequency of input signal and n the number of stages.

Differentiating equation 3.22 with respect to n gives an expression for the optimum number of stages.

For the equal value capacitor design:

$$N = \sqrt{(\frac{V_{max} fC}{2I_L})} \qquad 3.23$$

where N is the optimum number of stages.

The ripple voltage for all stage capacitances may be calculated from (Lux, 2001):

$$V_{ripple} = \frac{I_L}{(fC)} n \frac{(n+1)}{2} \qquad 3.24$$

Increasing the frequency reduces the ripple voltage and the voltage drop under load. The dc voltage generator normally includes a voltage inverter circuit to be able to generate the required voltage with an ac voltage source. Careful consideration of all component parameters is the only way to ensure reliable and predictable circuit performance.

3.2.2.2 Capacitor selection

The size of capacitors used in voltage multiplier circuit is inversely proportional to the frequency of the input signal. Capacitors used in off-line, 50Hz applications are usually in the range of 1 to 200μF while those used in higher frequency applications, say 10kHz and above, are typically in the range of 0.02 to 0.06μF. In practice, it is usually easier, and less expensive to use capacitors of the same value. The overall capacitive reactance of the circuit must be considered, however, to determine the largest permissible value. For the prototype to be constructed, high frequency switching method will be employed since the ripple associated with multiplier circuit varies inversely as the frequency of supply voltage and the capacitor values.

3.2.2.3 Rectifier selection

In the selection of the rectifier, the following parameters are considered:

Repetitive Peak Reverse Voltage (V_{RRM}) –The maximum allowable instantaneous value of reverse voltage across the rectifier diode. Application of reverse voltages below this maximum value will produce only negligible leakage currents through the diode while voltages in excess of this maximum value can cause permanent component damage. The V_{RRM} of diodes used will be at least twice the peak value of the voltage to be multiplied.

Reverse Recovery Time (t_{rr}) – This is a measure of the time needed for a rectifier diode to reach a state of complete blocking (I_R=0) upon the application of a reverse bias voltage. Ideally, this time should be zero but in reality it depends on the time it takes the stored charge at the diode junction to be "swept away"

before it can enter blocking mode. The stored charge is directly proportional to the forward current flowing through the junction prior to the application of the reverse bias voltage. The reverse recovery time is kept to a minimum since operating currents in voltage multiplier circuits are very low. The selected rectifier diode must be capable of switching at speeds faster than the rise and fall times of the input voltage for symmetrical signal inputs. If the reverse recovery time of the rectifier is too long, the efficiency and regulation of the circuit will suffer. In the worst case, insufficient recovery speeds will result in excessive device heating, as reverse power losses in the rectifier become significant.

Peak Forward Surge Current (I_{fsm}) - This is the maximum peak value of a single half-sine wave (50 or 60Hz) which, when superimposed upon the diodes rated load current (JEDEC method), can be conducted, without damaging the rectifier. This is important because surge currents can develop in multiplier circuits, due to capacitive loading effects. Usually significant surge currents can flow through the rectifiers during initial capacitor charging at turn-on. Series resistance is used to reduce the current surges. The value of R_s is calculated as follows:

$$R_s = \frac{V_m}{I_{fsm}} \qquad 3.25$$

where V_m is the peak value of the input voltage and I_{fsm} the peak surge current.

Forward current, I_o - In the ideal voltage multiplier circuit configuration, the load will draw no current. Significant amount of current only flows through the rectifiers during initial capacitor charging; therefore, devices with very low current ratings (hundreds of milliamperes) can be used.

Generally speaking, devices with a high surge current rating, I_{fsm}, will also have a high forward current, I_O, rating, and vice versa.

Forward Voltage, V_F - In practice, the forward voltage drop, V_F, of the rectifiers does not have a significant effect on the overall efficiency of the multiplier network.

The potential for high voltage sparks must also be considered as the value of n increases, and when higher output voltages are required. The selection of circuit components, however, is one aspect of the overall design that must not be trivialized as careful consideration of all component parameters is the only way to ensure both reliable and predictable circuit performance.

Figure 3.6 is the schematic diagram of an eight stage voltage multiplier circuit. The design is based on equal stage capacitance value with an expected output voltage of about 1.2kV. The voltage multiplier circuit is made up of a high frequency voltage oscillator circuit which serves as an input voltage to the primary winding of a step-up high frequency transformer. The changing magnetic field produced in the primary winding of the transformer by input voltage, then induces an emf in its secondary winding which is proportional to the inducing primary current. The induced secondary voltage is then multiplied by the diode – capacitor circuits. During the positive voltage half cycle of the induced secondary voltage, capacitor C3 charges to the peak value of the induced voltage through D1-D2. Capacitor C4 then charges to twice the peak value of the voltages developed across C3 and the transformer during the negative cycle of the

transformer secondary voltage through D3-D4 with C7 of the last stage of the multiplier circuit charging to $7V_p$.

3.3.1 Fabrication of the Vacuum Paper Hold-Down System

The developed vacuum hold down system consists of a dc motor-driven suction unit, a suction chamber, a perforated flat plotting surface and a pulse width modulated mctor speed controller.

3.3.1.2 The Suction unit

The suction unit was constructed from a 24 Volts DC blower purchased from a machine scrap market and it consists of 12° backward curved blade centrifugal fan impeller shown in figure 3.7.

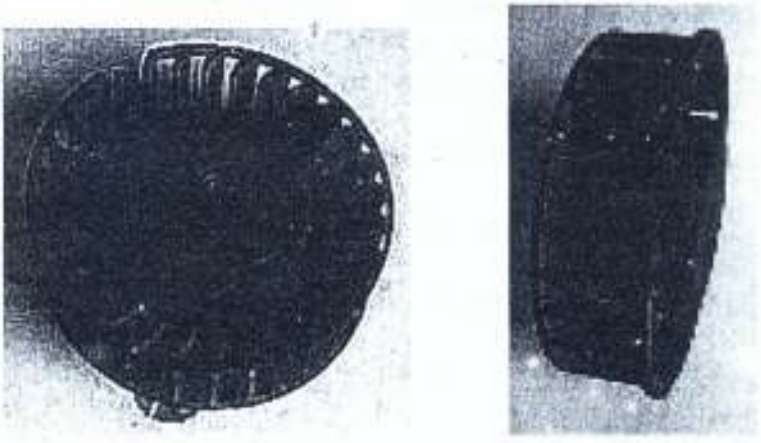

Fig 3.7 Photograph of the fan impeller with the DC motor

The dimensions of the backward curved angled blade centrifugal fan impeller are shown in table 3-1.

Table 3-1 Dimensions of the fan impeller.

Base diameter	90mm
Number of Blades	30
blade angle	12°
blade thickness	1.5mm
blade height	20mm
blade length	10mm
base thickness	2.5mm
impeller eye diameter	64mm

The air blower was converted to a suction unit by mounting its air inlet port onto a 15cm by 25cm flat wooden platform with central circular hole of 45mm diameter created with vertical milling machine (figure 3.8)

The hole in the wooden platform served as the air inlet port for the vacuum pump while the blowers air vent served as the pumps output port. The diameter of the inlet port (45mm) was determined by the centre eye of the centrifugal fan's impeller which was about 64mm. The smaller diameter helped in creating the required suction effect as the fan impeller rotates due to increased air velocity pressure at the inlet port (Bernoulli's principle). The effective suction pressure also depends on the speed of the fan motor, the blade angle, the number of blades as well as the duct size of the perforated aluminum sheet.

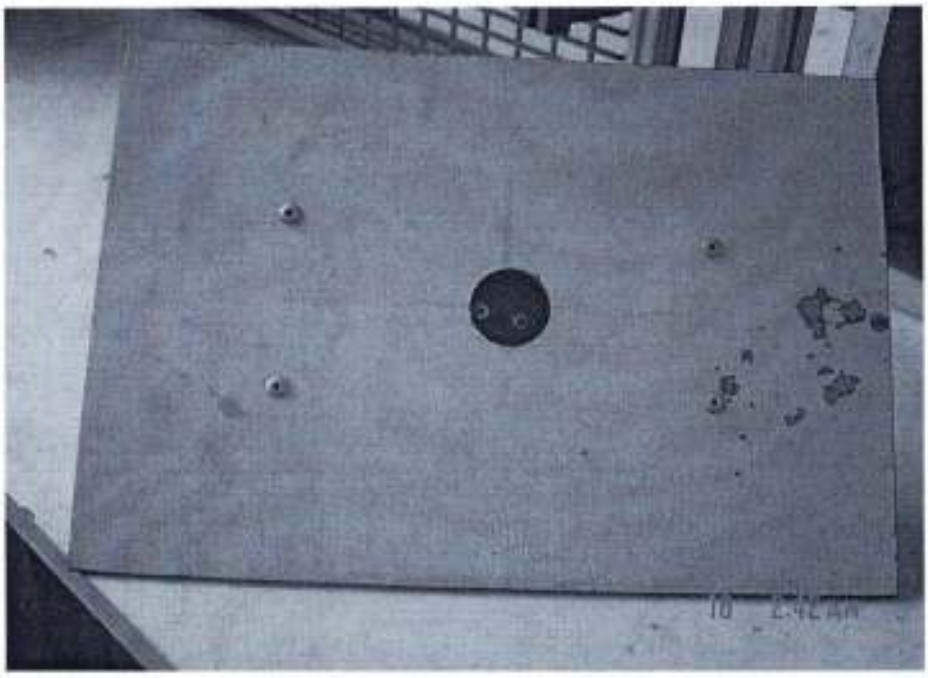

Fig 3.8 Photograph of the suction pump showing the wooden platform and the air inlet port .

3.3.1.3 The Suction Chamber

The suction chamber was constructed using a rectangular PVC plastic material to create an air gap of about 1.5cm diameter between the 42cm by 21cm perforated aluminum sheet and the wooden platform of the suction unit. The perforations on the flat aluminum sheet were created using 1mm diameter drilling bits of a milling machine.

The rectangular PVC plastic electrical cable trunking pipe was glued onto the perforated aluminum sheet using silicon glue gum. The gum was also used to couple the wooden platform of the suction unit. The created air suction chamber has a dimension of 20cmx15cmx1.5cm. The dc motor driven suction unit and the suction chamber make up the vacuum pump.

3.3.1.4 The pulse-width-modulated motor speed controller

The design of the speed controller was based a fixed-frequency pulse-width-modulated (PWM) voltage-regulator control circuit SG3525 from Signetics, Texas Instruments. The schematic circuit diagram figure 3.9 was first assembled on a bread board and its functionality was confirmed using bench power supply and oscilloscope before the components were soldered onto a universal printed circuit board. The circuit operates at a fixed frequency of about 100 Hz set by resistors R4 - VR2 and capacitor C3. R4-VR2 establishes a constant charging current for C3 as well as the operating frequency for speed control circuit given by (Texas instruments, 2003): The expression for the frequency was obtained from the components manufacturers' data sheet.

3.3.1.3 The Suction Chamber

The suction chamber was constructed using a rectangular PVC plastic material to create an air gap of about 1.5cm diameter between the 42cm by 21cm perforated aluminum sheet and the wooden platform of the suction unit. The perforations on the flat aluminum sheet were created using 1mm diameter drilling bits of a milling machine.

The rectangular PVC plastic electrical cable trunking pipe was glued onto the perforated aluminum sheet using silicon glue gum. The gum was also used to couple the wooden platform of the suction unit. The created air suction chamber has a dimension of 20cmx15cmx1.5cm. The dc motor driven suction unit and the suction chamber make up the vacuum pump.

3.3.1.4 The pulse-width-modulated motor speed controller

The design of the speed controller was based a fixed-frequency pulse-width-modulated (PWM) voltage-regulator control circuit SG3525 from Signetics, Texas Instruments. The schematic circuit diagram figure 3.9 was first assembled on a bread board and its functionality was confirmed using bench power supply and oscilloscope before the components were soldered onto a universal printed circuit board. The circuit operates at a fixed frequency of about 100 Hz set by resistors R4 - VR2 and capacitor C3. R4-VR2 establishes a constant charging current for C3 as well as the operating frequency for speed control circuit given by (Texas instruments, 2003): The expression for the frequency was obtained from the components manufacturers' data sheet.

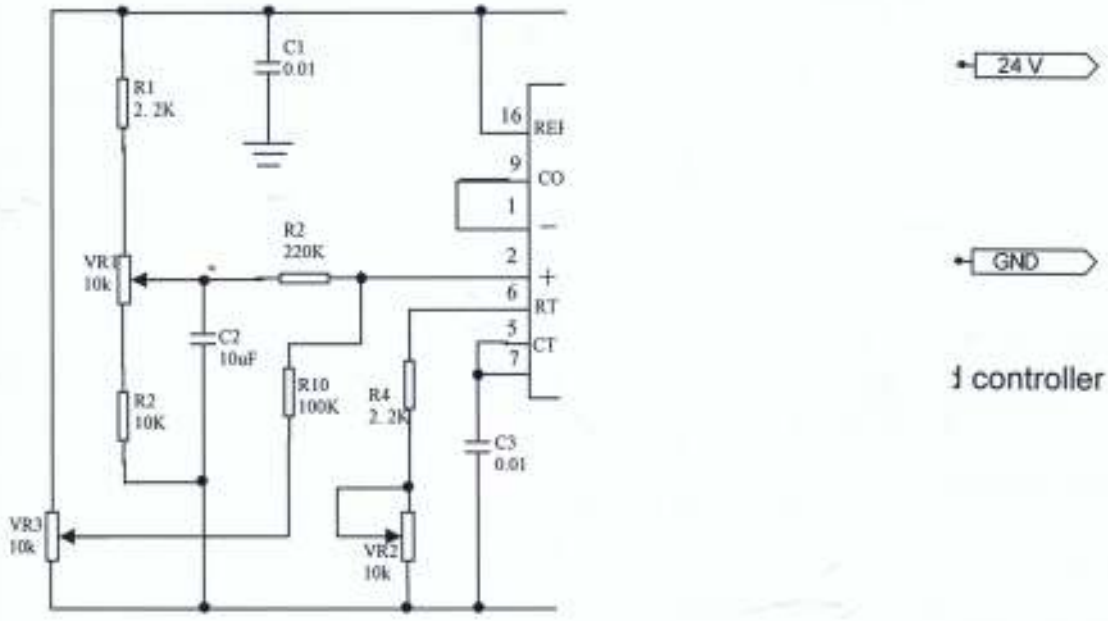

Fig. 3.9 Circuit diagram of the PWM mo

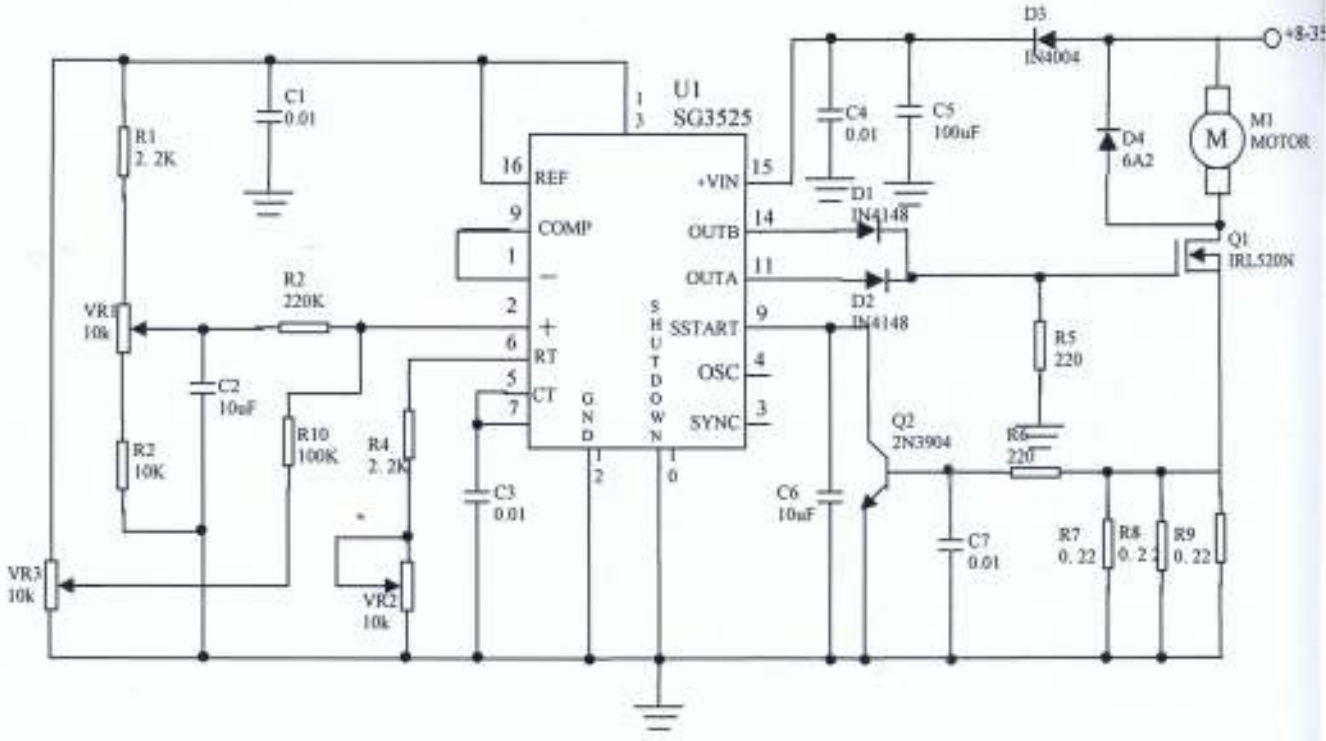

Fig. 3.9 Circuit diagram of the PWM motor speed controller

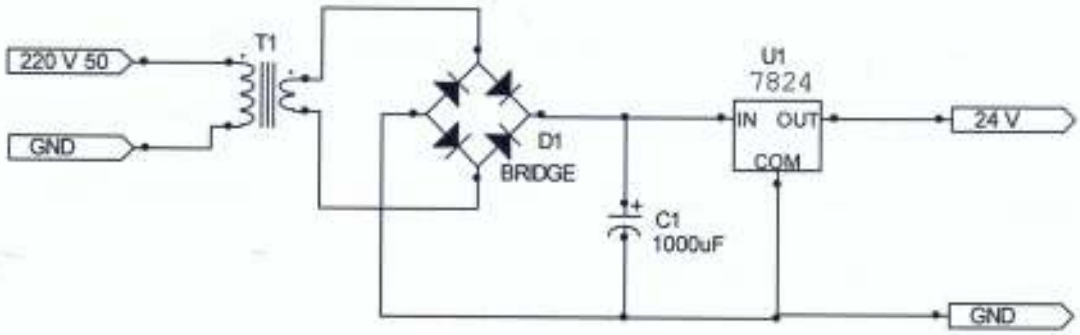

Fig. 3.10 Circuit diagram of the regulated power supply for the speed controller

The different sections were then coupled together to form the vacuum hold down system. For varying pump speed, the constructed unit was then used under laboratory condition to measure the hold-down force for A3 sized paper of different gauges using gravitational force technique. The aim of the laboratory test was to establish the relationship between suction pressure and the speed of the fan's impeller while under the control of the speed controller.

The minimum weight required to slide the plotting paper across the plotting surface while under the influence of vacuum pump was measured for varying pump speed. A weighed scale pan was attached to the plotting paper by means of two light inextensible strings and two small sized frictionless pulleys (2.5cm diameter) mounted by the side of the aluminum housing of the vacuum hold-down system as shown in figure 3.11.

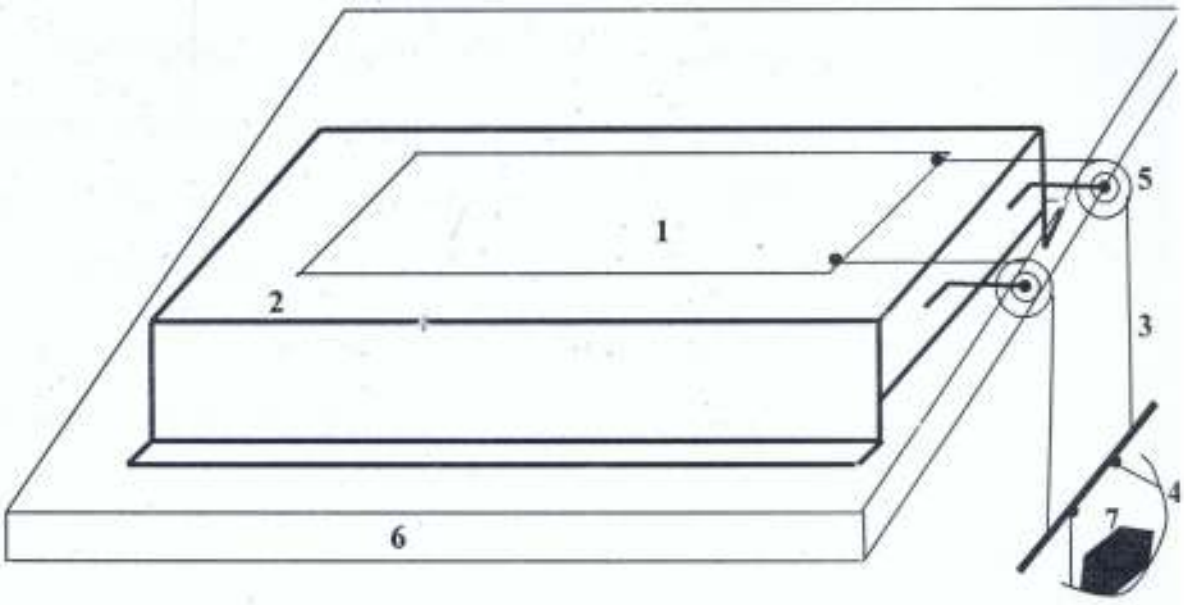

Fig 3.11. Diagram of the laboratory measurements setup.

1. Plotting paper 2. Plotting surface 3. String 4. Scale pan

5. Pulley system 6. workbench 7. Weight

Weights were then added to the scale pan until the paper began to slide across the surface of the perforated aluminum sheet. The total mass was recorded for different pump speed. The pump speed was measured with an optical tachometer by measuring the rotation of the fan impeller in revolution per minute. A digital multimeter served as an output device for the optical tachometer. The values of the measured speed were obtained in millivolts and converted to revolutions per minute using a conversion table provided by the instrument manufacturers (1mV equals 10 rpm).

3.3.2.0 The Electrostatic paper hold-down system

The electrostatic hold down system consists of three major parts separately designed, constructed and coupled together to form a complete unit. The parts were the;

- Electrostatic charging unit (DC high voltage supply)
- Charging plate
- Flat aluminum plotting surface

3.3.2.1 The charging plate

Two charging units were constructed using corona discharge model and parallel plate capacitor model.

Parallel Plate Capacitor model

Two flat aluminum sheets (30cmx20cmx0.5cm) separated by a mica sheet (Formica) as the dielectric material were glued together using aevostick adhesive gum as shown in fig 3.12.

Two electrical terminals were provided for the connection to the high voltage supply unit. The outer surfaces of the aluminum plates were insulated with transparent polyester material to act as safety measure against electric shock. The constructed charging unit was attached to the lower surface of the flat plotting table with aevostick adhesive gum to charge the plotting table. The plotting table shown in figure 3.13 is made of aluminum sheet with dimensions 42cm by 21cm by 7.5cm. The dimensions for the plotting table were chosen for an A3 sized plotting paper. The upper surface of the plotting table was also insulated with transparent polystyrene.

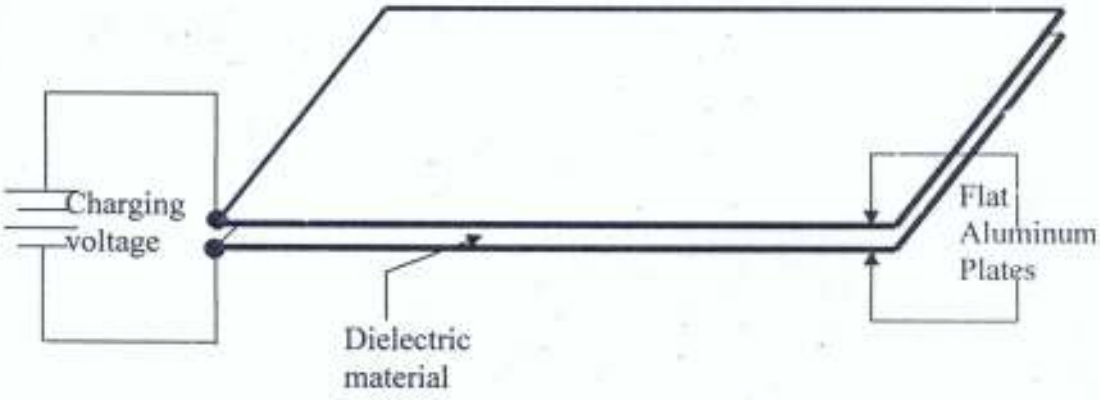

Fig. 3.12 Diagram of the capacitor charging model

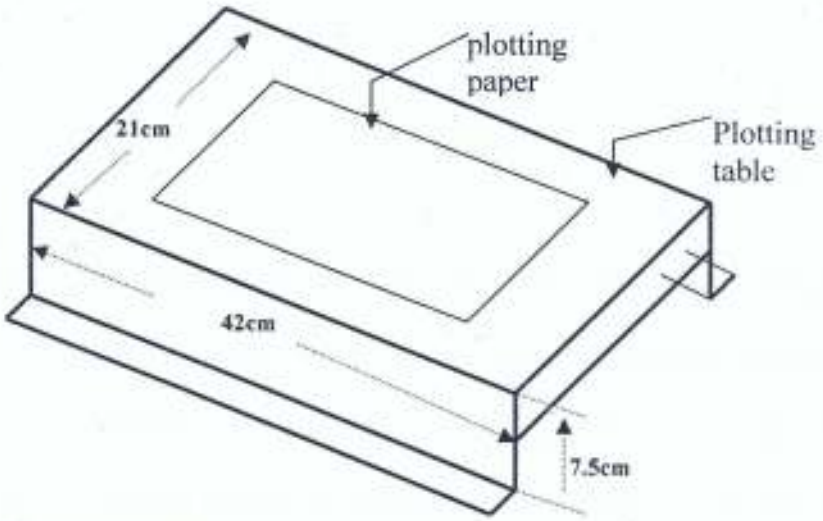

Fig 3.13 The plotting table

3.3.3 Corona charging model

Two pieces of white pvc plastic sheets were attached to the two ends of a rectangular sized aluminium plate (30m by 2cm by 1mm) with the help of a quick set epoxy gum. A 0.3mm tungsten wire was then used as a set of six parallel corona discharge electrodes. The aluminium plate insulated on both sides with mica (Formica) served as the charging plate when the high voltage supply is connected between it and the corona electrodes.

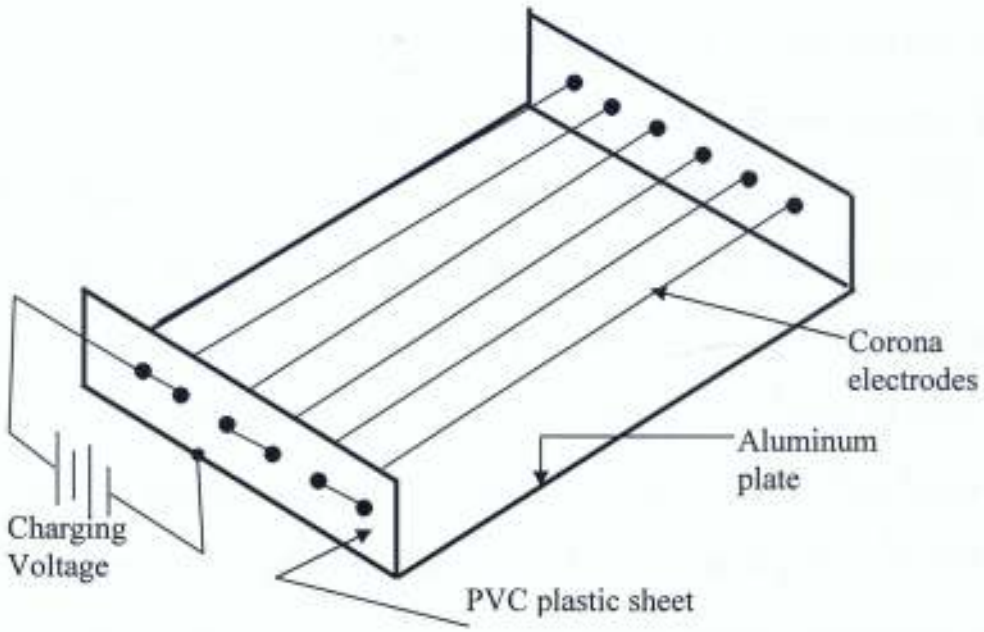

Fig 3.14 Diagram of the corona charging unit

The constructed corona charging unit was then adhered to the lower surface the plotting table with the insulated upper surface to form another electrostatic hold down. Electrical connection terminal were provided for the connection of the high voltage charger by means electrical connectors connected to the aluminum plate and the corona electrodes.

The constructed electrostatic unit was then used to hold the A3 sized paper of different gauges while varying the charging voltage supplied from the high

voltage supply unit. The variation of the charging voltage with the force between the plotting surface and the paper was studied and the relationship between the hold-down force and the charging voltage was obtained from the collected data using the regression equation.

3.3.4 DC High Voltage Charge Generator

The design of the electrostatic charge generator was based the voltage multiplication principle using the normal (half wave) symmetrical Cockcroft-Walton voltage multiplier circuit a (modified Jacob's ladder voltage multiplier circuit). The circuit is fed from a 0-30 volt adjustable dc power supply. The input to the multiplier circuit was provided using a step-up DC-to-AC voltage inverter circuit. The DC-to-AC voltage inverter is made up of six Schmitt trigger inverting gates U1A-U1F. Gate U1A is used as a square wave generator with oscillating frequency of 12 kHz. The output of U1A is fed to the inputs of U1B to U1F, connected in parallel to boost the drive current for the switching transistor Q1. The square wave output of the gates connected in parallel is fed to the base of Q1, causing it to switch ON and OFF continuously thereby passing an ac current through the primary winding of a step-up high frequency transformer T1. This produces a changing magnetic field in the primary winding of T1 that induces a pulsating output voltage of 500-volts, 12 kHz at the secondary winding of T1. The pulsating DC output at the secondary winding of T1 is then applied to an 8-stage voltage-multiplier circuit to produce an output voltage of about to 1,200-volts DC. The schematic diagram of the generator is shown in figure 3.15 while that of the adjustable dc voltage source is in figure 3.16.

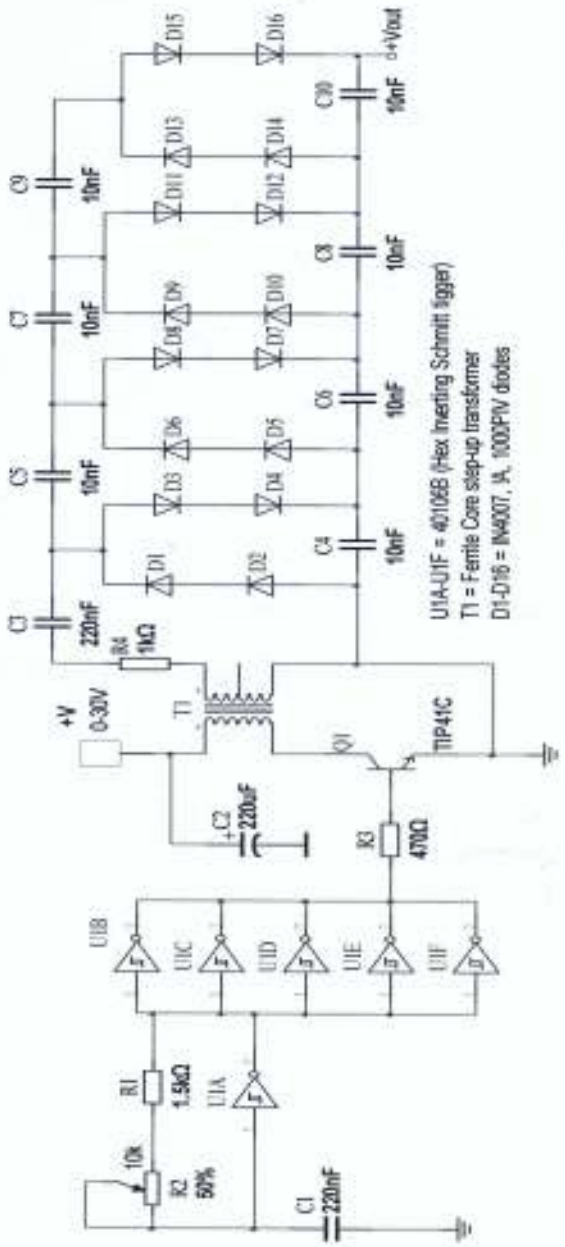

Fig 3.15 Complete schematic diagram of charge generator

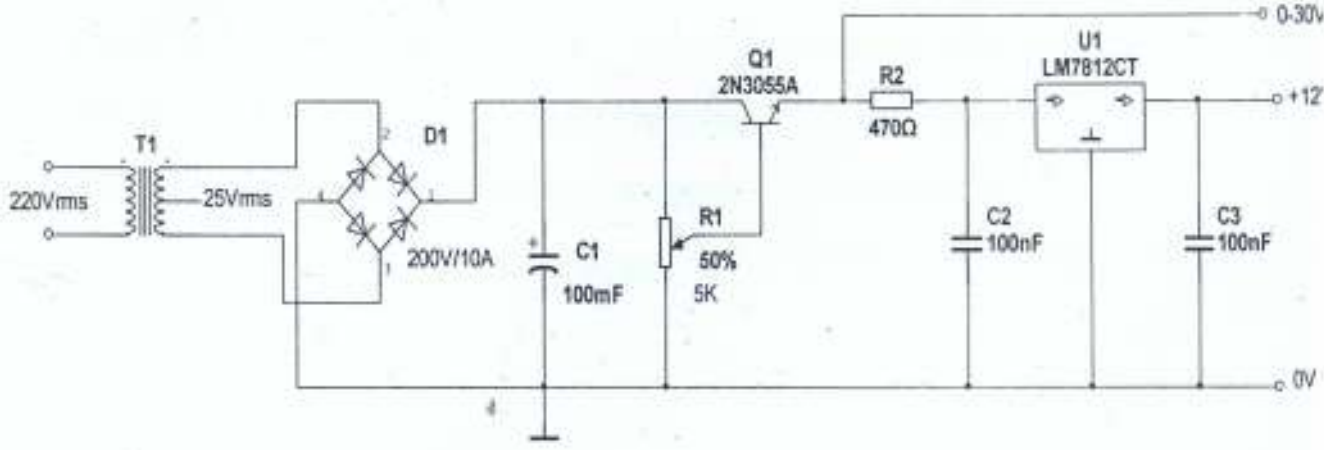

Fig. 3.16 Schematic diagram of the adjustable dc voltage source

Before assembling the circuit on a printed circuit board, software simulation of the circuit was done using national instrument's electronic workbench Multisim 10.0. Figure 3.17 shows the output waveform of oscillator unit of the dc to dc up converter used as the ac voltage source for the voltage multiplier circuit displayed using an analogue oscilloscope. The figures are snapshots of oscilloscope screen taking with a digital camera.

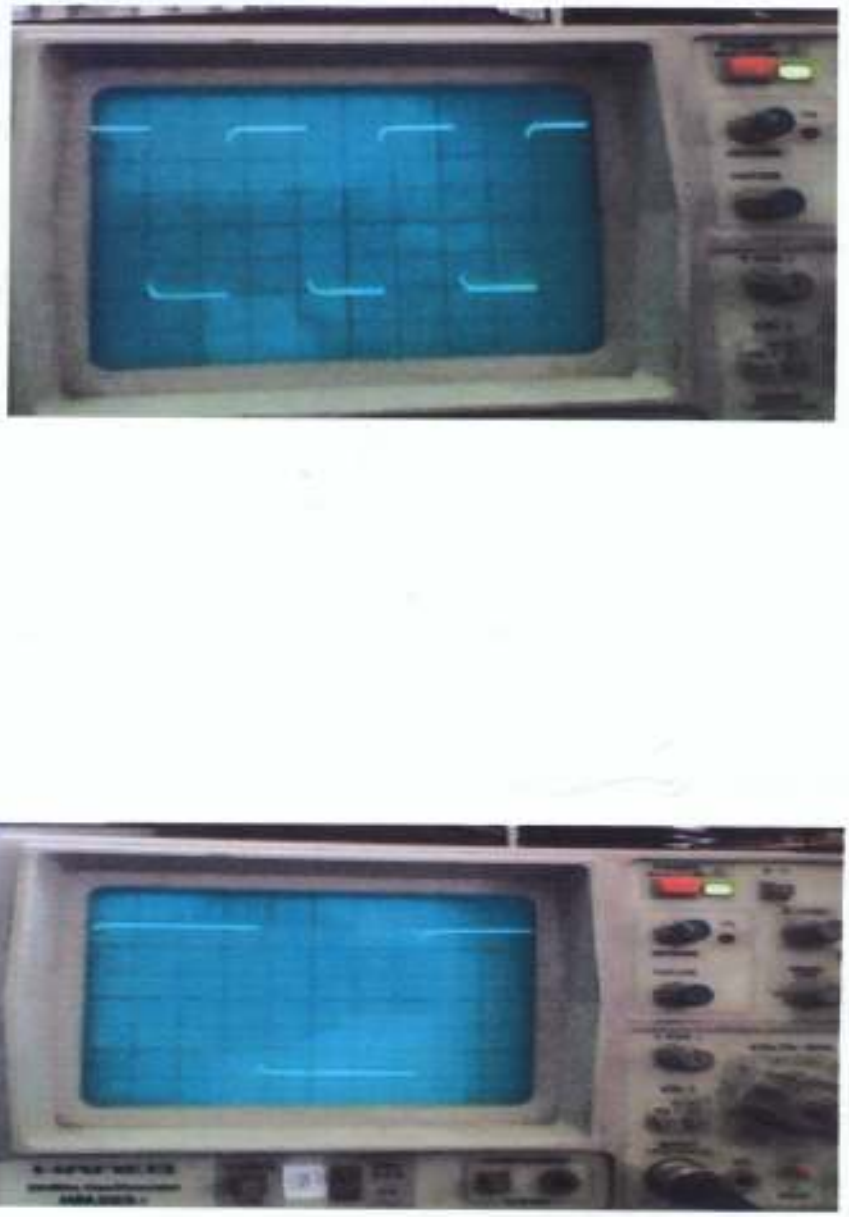

Fig. 3.17 Photographs of the Oscilloscope display of the inverter oscillator output Waveform for different time base settings

Laboratory experiment was also carried out to determine the coefficient of static friction between the plotting surfaces and the plotting paper. The minimum angle of inclination of the plotting surface at which the plotting paper began to slide down the inclined surface was measured using steel meter rule. The force analysis diagrams for the experiment are shown in figure 3.18.

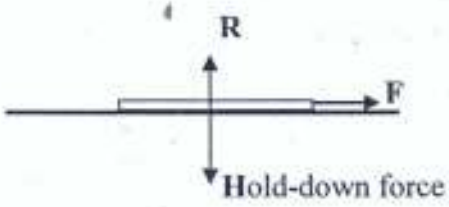

R is the vertical upward reaction force on the plotting table due the weight of the plotting paper

F is the horizontal sliding force applied to the plotting paper while under the influence of the hold-down force action vertically downwards.

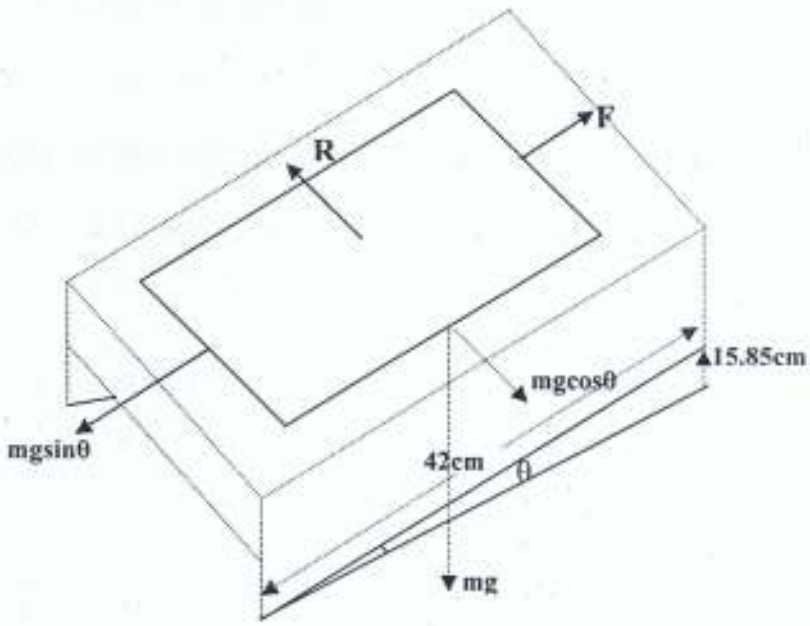

Fig. 3.18 the force analysis diagrams

CHAPTER FOUR

4.0 Results and Discussion

4.1 Results for the Vacuum hold-down system

The laboratory test results obtained from the measurements are presented in tables 4.1 and 4.2 for the vacuum paper hold-down. The optical tachometer readings in millivolts are shown in column 2 of the tables. The recorded values were converted to speed in revolutions per minute using the conversion factor provided by the instrument manufacturer. The hold-down force, was calculated using equation 4.1

$$Hold-down\ force = \frac{F}{\mu} \qquad 4.1$$

μ is the coefficient of static friction between the plotting paper and the plotting surface, and F is the minimum horizontal force that slides the plotting paper across the plotting surface

The coefficient of static friction for the system is derived using data obtained from figures 3.18 and 3.19 of the force analysis diagrams:

$$\mu = \tan\theta$$

Where θ is the angle of inclination of the system and is given as:

$$\theta = \sin^{-1}\frac{15.85}{42}$$
$$= 22.2^{0}$$

Therefore the coefficient of static friction is:

$$\mu = \tan 22.2^{0}$$
$$= 0.41 \pm 0.02$$

Graphical representations of the data are presented in figures 4.1 and 4.2 respectively. The slope of the graphs obtained from the regression analysis tables 4.3 and 4.4 showed that the average hold-down force for the vacuum paper hold-down system is 0.001 ±N per 100rpm for the cardboard sheet and 0.004 ± 0.0001N per 100rpm for the 80gsm paper.

Table 4.1 Experimental data for A3 sized cardboard paper sheet for the vacuum paper hold-down system

S/N	Tachometer reading in mV	Impeller speed in rpm	Mass (gf)	Sliding force F in N	Hold-down force(N)=F/μ
1	162	1620	33.3	0.33	0.80
2	181	1810	37.1	0.37	0.92
3	204	2040	41.6	0.45	1.10
4	230	2300	51.2	0.51	1.24
5	280	2800	66.2	0.65	1.59
6	325	3250	89.0	0.87	2.12
7	357	3700	98.0	0.97	2.37

Table 4.2 Experimental data for A3 sizes 80gsm sheet for paper the vacuum paper hold-down system

S/N	Tachometer reading in mV	Impeller speed in rpm	Mass (gf)	Sliding force F in N	Hold-down force(N)=F/μ
1	195.9	1959	23.3	0.23	0.56
2	221.0	2210	30.6	0.31	0.76
3	253.0	2530	36.1	0.36	0.88
4	282.0	2820	38.1	0.38	0.93
5	322.0	3220	45.6	0.46	1.12
6	360.0	3600	50.6	0.51	1.24
7	401.0	4010	61.4	0.61	1.49

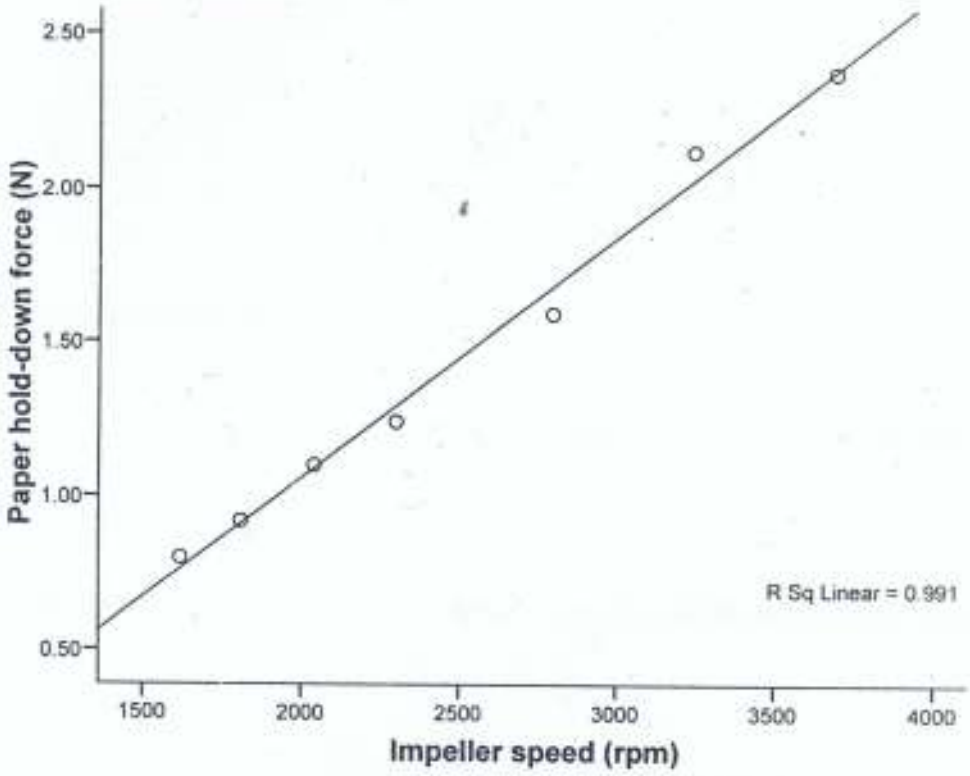

Fig. 4.1 Paper hold-down force against pump impeller speed for A3 sized cardboard paper

Table 4.3 Regression Analysis Result for the vacuum paper hold-down system on A3 sized cardboard plotting paper

	Estimated coefficients	Standard error
m	0.004	0.001
c	-0.208	0.075

The regression equation is given as

$$y = mx + c \qquad 4.1$$

Where y is the hold-down force of the system, m the slope and the intercept of the slope on the vertical (hold-down force) axis.

The regression equation for the estimation of the paper the estimation hold-down force for system is derived as follows:

$$Hold-down\ force\ (F) = m \times impeller\ speed\ (I_s) + c$$

Whereby the derived regression equation is:

$$F = 0.004 I_s - 0.208 \qquad 4.2$$

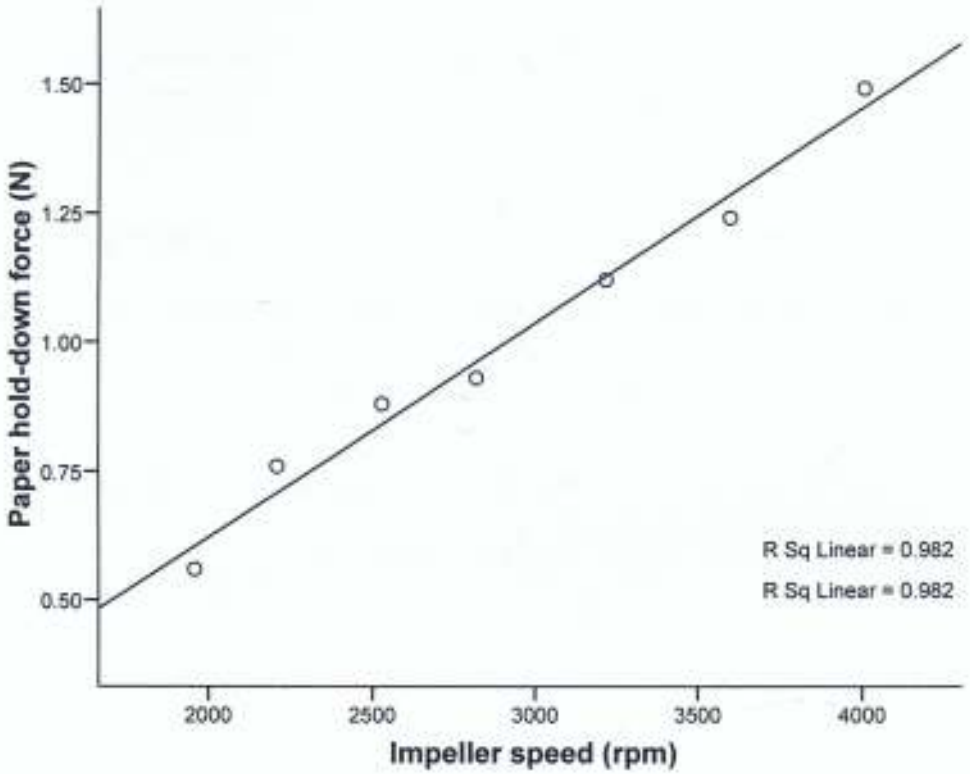

Fig. 4.2 Paper hold-down force against impeller speed for A3 sized 80gsm paper.

Table 4.4 Regression analysis result for the vacuum paper hold-down system on A3 sized 80g plotting paper

	Estimated coefficients	Standard error
m	0.001	0.0001
c	-0.494	0.088

The regression equation for the estimation of the paper the estimation hold-down force for the vacuum system for 80g paper is derived as follows:

$$Hold-down\ force\,(F) = m \times impeller\ speed\,(I_s) + c$$

Whereby the derived regression equation is:

$$F = 0.001 I_s - 0.208 \qquad 4.3$$

4.2 Results for the electrostatic hold-down system

For the electrostatic paper hold-down system, the experimental results are as presented in table 4.5 while the graphical representation of the data is presented in figure 4.3. The slope of regression analysis table 4.6 showed that the average hold-down force for the electrostatic hold-down system for an 80gsm plotting paper is 0.003 ± 0.0001 N per volt.

Table 4.5 The experimental results for electrosiatic paper hold-down system for an 80gsm A3 sized plotting paper.

S/N	Applied Charging Voltage (V)	Mass (gf)	Sliding force in N	Hold-down force(N)=F/μ
1.	100	5.20	0.05	0.12
2.	300	46.60	0.46	1.12
3.	500	69.40	0.68	1.66
4.	700	82.50	0.81	1.96
5.	900	105.30	1.03	2.51
6.	1100	151.20	1.48	3.61
7.	1300	185.20	1.82	4.43

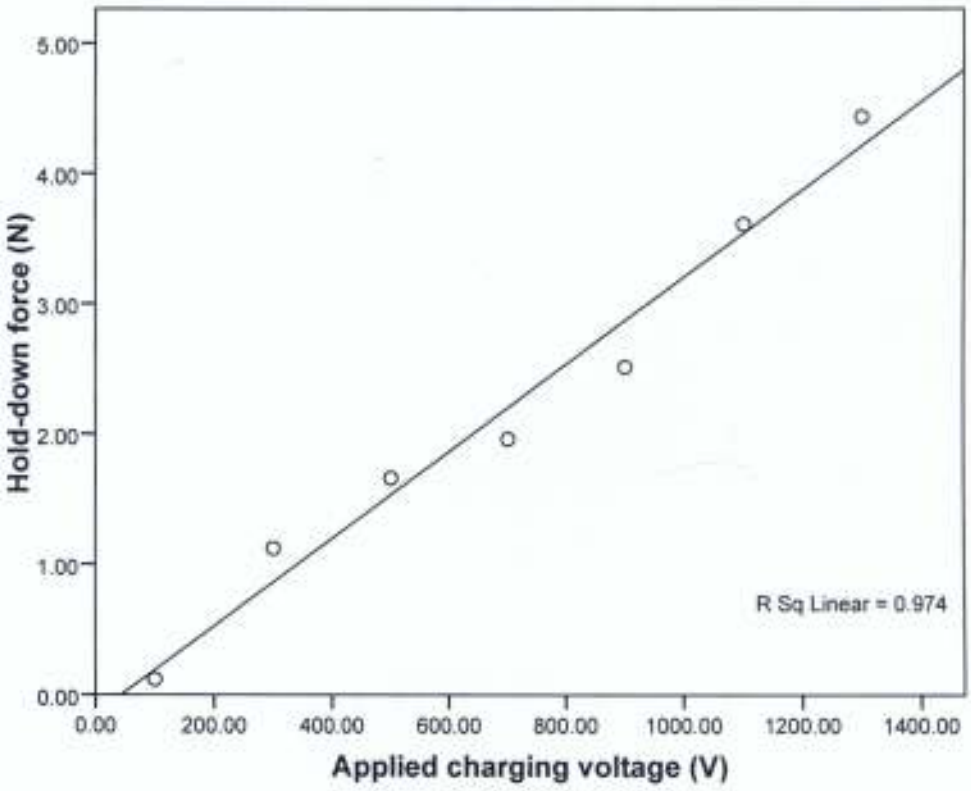

Fig.4.3 Paper hold-down force against applied charging voltage for 80gsm A3 sized plotting paper.

Table 4.6 Regression Analysis Result for the Electrostatic Paper hold-down system on A3 sized 80g plotting paper

	Estimated coefficients	Standard error
m	0.003	0.0002
c	-0.144	0.196

The regression equation for the estimation of the paper the estimation hold-down force for system is derived as follows:

$$Hold-down\ force\ (F) = m \times applied\ charging\ voltage\ (V_c) + c$$

Whereby the derived regression equation is:

$$F = 0.003V_c - 0.144 \qquad 4.4$$

4.3 Limitation of Results

The degree of accuracy obtained in the hold-down force for the developed paper hold-down systems are the errors associated with estimation of the coefficients of the regression analysis as indicated in tables 4.3, 4.5 and 4.6 respectively.

For the vacuum hold-down system, the percentage error for the hold-down force for 80g paper is:

$$\%error = \frac{0.0001}{0.001} \times 100$$
$$= 10\%$$

For the A3 sized cardboard paper, the estimated percentage error is:

$$\%error = \frac{0.0001}{0.004} \times 100$$
$$= 3.3\%$$

The estimated error for the electrostatic paper hold-down system for the 80g paper is:

$$\%error = \frac{0.0002}{0.003} \times 100$$
$$= 6.7\%$$

4.4 DISCUSSION

The vacuum hold-down system

The computed hold-down force was derived considering the minimum weight (horizontal force) able to slide the paper across the aluminum surface and the coefficient of static friction between the plotting table and the paper. These represented the temporary adhesive force that held the paper on the plotting table under the influence of the paper hold down systems. The average hold-down force per rpm, generated by the vacuum system for A3 80gsm sized paper varied as indicated by the slope of the regression analysis which is 0.004± 0.0001N per 100rpm and 0.001± 0.0001N per 100rpm for the A3 sized cardboard paper. Detail of the regression analysis on the experimental data is in appendix B. The plotted graphs showed a linear relationship between the hold-down force and the impeller speed as expressed by the regression equations 4.1 and 4.2 respectively.

The electrostatic hold-down system

For the electrostatic hold-down system the generated hold down force varied as the applied charging voltage. A graph of hold-down force against the charging voltage also produced a linear relationship with an average hold-down force of 0.003±0.0002N per volt as by the slope of the regression analysis of the experimental data.

4.5 CONCLUSION

The results indicate that the two systems under study were efficient as paper hold down systems but the vacuum system is more bulky requiring additional hardware for its implementation. The charging system of the electrostatic hold down system can be implemented as part of the power supply section of the XY plotter. This reduces the hardware requirement for its implementation. In terms of operational hazards, the vacuum system is more user-friendly. The high voltage system used as charge generator for the electrostatic hold-down system requires the use of electrical insulators around the plotting table to reduce the risk of electric shock. In all, the objective of the study was achieved in providing practical paper hold down systems for XY plotters.

References

Avallone E.A and Baunmeister T (1987); Mark's Standard Handbook for Mechanical Engineers, 9th Edition, McGraw-Hill, Inc. New York, pg. 14-48

Basics of Electrostatic Discharge, Copyright 1999-2003, ESD Association 7900 Turin Road, Building 3 Rome, NY 13440-2069 USA

Bodman G. R, and Shelton D. P. (1996); Ventilation Fans: Types and Sizes. University of Nebraska: NebGuide. [online textfile]. Retrieved November 22, 2004 from http://ianrpubs.unl.edu/farmbuildings/g1243.htm

Bruce D.W and James K.R (1969); Electronic Components and Measurements, Prentice-Hall, Inc., Englewood Cliffs, N.J

Cornish J.J (1987); Aeronautics, Marks Standard Handbook for Mechanical Engineers, 9th Edition, McGraw-Hill, Inc. New York, pg. 11-69

Coste J and Pechery P (1981); Influence of surface profile in polymer-metal contact charging, journal of Electrostatics 10 129-136

Cross J. A (1987); Electrostatic principles, problems and applications, Bristol Adam Hilger

Davies D.K (1969); Charge generation on dielectric surfaces, J Phys. D: Applied Physics 2, 1533-1537

Doebelin E. O (1990); Measurement System Application and Design, 4th

Edition, McGraw Hill Publishing Company New York

Electrostatic Charging; [online textfile]. Retrieved from;

http://www.cartage.org.lb/en/science/physics/mainpage.htm

Electrostatic Discharge (ESD), (2005); [online textfile]. Retrieved from

www.Semiconfareast.com

Griffiths D. J. (1998). Introduction to Electrodynamics 3rd edition,

Prentice Hall.

Greason W. D (1987); Electrostatic Damage in Electronic Devices and

Systems, Research Studies Press Ltd, 24 Belvedina Road Taunton,

Sonerset England Tauhd pg. 45-49.

Gudavalli S., Atul Mittai and Sangeeta Nangia; Energy Efficiency FRP Axial

Flow Fans. [Online Text file]. Retrieved from

http://www.tifac.org.in/newlett.htm

Haslam J.A, Summers G.R & Williams D (1993); Engineering Instrumentation

and Control, British Library Cataloguing in publication Data

Haenan HTM (1976); Experimental investigation of relationship between

generation and decay of charges on dielectrics, Journal of Electrostatics 2

151-173

Harris T. (2005); How Vacuum Cleaners Works, [Online Text file] Retrieved

From http://www.howstuffworks.com

Jonassen N (2000); "Polarization, for Better or Worse," in Mr. Static, Compliance Engineering 17, no. 5 pg. 34–40

Jonassen N (2000); How is Static Electricity Generated, [Online Text file] Retrieved from http://www.ce-mg.com

Laycock C.H (1976), Applied Electro technology for Engineers, 1st Edition, Macmillan Press

Lux J (2001); Cockroft Walton voltage multiplier, [Online Text file] Retrieved from http://home.earthlink.net/jimlux/index

McPherson M. J (1993); Subsurface Ventilation and Environmental Engineering, London, New York, Chapman and Hall, TN301.M37

Michel J. (2005); Cockroft-Walton Optimum design guide V2.0, Retrived from http://www.blazelabs.com

Morris N. M. (1987); Control Engineering, 3rd Edition, McGraw-Hill Book Company (UK) Ltd. London

Montgomery D. J (1959); Contact electrification in solids, journal of solid state phy. Vol. 9, pp. 139-197

Ohara K. (1979); Contribution of molecular motion of polymers to frictional

From http://www.howstuffworks.com

Jonassen N (2000); "Polarization, for Better or Worse," in Mr. Static, Compliance Engineering 17, no. 5 pg. 34–40

Jonassen N (2000); How is Static Electricity Generated, [Online Text file] Retrieved from http://www.ce-mg.com

Laycock C.H (1976), Applied Electro technology for Engineers, 1st Edition, Macmillan Press

Lux J (2001); Cockroft Walton voltage multiplier, [Online Text file] Retrieved from http://home.earthlink.net/jimlux/index

McPherson M. J (1993); Subsurface Ventilation and Environmental Engineering, London, New York, Chapman and Hall, TN301.M37

Michel J. (2005); Cockroft-Walton Optimum design guide V2.0, Retrived from http://www.blazelabs.com

Morris N. M. (1987); Control Engineering, 3rd Edition, McGraw-Hill Book Company (UK) Ltd. London

Montgomery D. J (1959); Contact electrification in solids, journal of solid state phy. Vol. 9, pp. 139-197

Ohara K. (1979); Contribution of molecular motion of polymers to frictional

electrification, IOP conference ser. No 48, pp. 257-264

Turner M and Rotron C (2004); All You Need to know about Fans, Online textfile http://www.rotron.com

Reinhold G. and Gleyvod R. (1975); Megawatt HV DC power Supply, IEEE Transactions on nuclear science, Vol. ns.22, no.3, June 1975

Robert J (1987); Fan Engineering, 8th Edition, Buffalo forge company

Sofasco; Fan Characteristics (AC-DC cross flow fans), [Online Text file] Retrieved from http://www.sofasco.com/Index.htm

Taylor D.M & Secker P.E (1994); Industrial Electrostatics: Fundamentals and Measurements, Research Studies Press Ltd. Taunton, Somerset, England

The Bakkan Library and Meseum; The Science of static Electricity, [Online text file]. Retrieved from; http://www.thebakken.org/library

Vent-Axia Ventilation Handbook-Fan Characteristics Curves, [Online Text file]. Retrieved from http://www.vent-axia.com

Vinson J.E and Liou J.J (1998); Electrostatic Discharge in Semiconductors, Proceedings of the IEEE, vol. 86, no. 2

Vyverberg R.G (1965); Xerography and Related processes, Dessauer JH and clark HE eds, Newyork facal

Zimmer E. (1970); Electrostatic charging of high-polymer insulating materials, Kunstoffe, vol. 60, pp. 465-468

Table A1: The Triboelectric Series for electrostatic chargeable materials

Most Positive (+)	
Air	+ + +
Human Hands, Skin	
Asbestos	
Rabbit Fur	
Glass	
Human Hair	
Mica	
Nylon	
Wool	
Lead	
Cat Fur	
Silk	
Aluminum	
Paper	
Cotton	+
Steel	
Wood	
Lucite	-
Sealing Wax	
Amber	
Rubber Balloon	
Hard Rubber	
Mylar	
Nickel	
Copper	
Silver	
uv Resist	
Brass	
Synthetic Rubber	
Gold, Platinum	
Sulfur	
Acetate, Rayon	
Polyester	
Celluloid	
Polystyrene	
Orlon, Acrylic	
Cellophane Tape	
Polyvinylidene chloride (Saran)	
Polyurethane	
Polyethylene	
Polypropylene	
Polyvinylchloride (Vinyl)	
Kel-F (PCTFE)	
Silicon	
Teflon	
Silicone Rubber	- - -
Most Negative (-)	

APPENDIX B1

Regression analysis Results

Regression equation is given as:

$$y = mx + c$$

$$Slope\ error = \sqrt{\frac{\sum (y-\bar{y})^2 - \frac{\left[\sum (x-\bar{x})(y-\bar{y})\right]^2}{\sum (x-\bar{x})^2}}{n-2}}$$

Table B1 80gsm paper (vacuum hold-down system)

Model Summary

Model	R	R Square	Adjusted R Square	Std. Error of the Estimate
1	.991(a)	.982	.979	.04565

Predictors: (Constant), Impeller speed (rpm)

Regression Coefficients

Model		Unstandardized Coefficients		Standardized Coefficients	t	Sig.
		B	Std. Error	Beta	B	Std. Error
1	(Constant)	-.208	.075		-2.782	.039
	Impeller speed (rpm)	.004	.0001	.991	16.569	.000

Dependent Variable: Paper hold-down force (N)

Table B2 cardboard paper (vacuum hold-down system)

Model Summary

Model	R	R Square	Adjusted R Square	Std. Error of the Estimate
1	.995(a)	.991	.989	.06411

Predictors: (Constant), Impeller speed (rpm)

Regression Coefficients

Model		Unstandardized Coefficients		Standardized Coefficients	t	Sig.
		B	Std. Error	Beta	B	Std. Error
1	(Constant)	-.494	.088		-5.606	.002
	Impeller speed (rpm)	.001	.0001	.995	22.948	.000

Dependent Variable: Paper hold-down force (N)

Table B3 80gsm paper (electrostatic hold-down system)

Model Summary

Model	R	R Square	Adjusted R Square	Std. Error of the Estimate
1	.987(a)	.974	.969	.25686

Predictors: (Constant), Applied charging voltage (V)

Regression Coefficients

Model		Unstandardized Coefficierts		Standardized Coefficients	t	Sig.
		B	Std. Error	Beta	B	Std. Error
1	(Constant)	-.144	.196		-.734	.496
	Applied charging voltage (V)	.003	.0001	.987	13.802	.000

Dependent Variable: Hold-down force (N)